2015

ENHANCED NANOPORE DETECTION VIA DIFFUSION GRADIENTS AND OPTICAL TWEEZERS

Kyle T. Brady
Virginia Commonwealth University

ENHANCED NANOPORE DETECTION VIA DIFFUSION GRADIENTS AND OPTICAL TWEEZERS

A thesis submitted in partial fulfillment of the requirements for the degree of Master of Science in Physics and Applied Physics at Virginia Commonwealth University.

by

Kyle Timothy Brady

B.S., Physics, Virginia Commonwealth University, 2013
B.S., Chemistry, Virginia Commonwealth University, 2013
M.S., Physics and Applied Physics, Virginia Commonwealth University, 2015

Director: Joseph Reiner, Ph.D., VCU Physics Department

Virginia Commonwealth University
Richmond, Virginia
May, 2015

Vita

Kyle Timothy Brady was born on February 11, 1990, in Virginia Beach, Virginia, and is an American citizen. He graduated from Kempsville High School, Virginia Beach, Virginia in 2008. He received his Bachelor of Science degrees in Physics and Chemistry from Virginia Commonwealth University, Richmond, Virginia in 2013.

Dedication

This work is dedicated to my wife and my parents, who never stopped supporting me throughout my college years.

Acknowledgement

I would like to thank Dr. Joseph Reiner for the help and expertise provided in coming up with and researching my thesis topics.

Table of Contents

List of Figures

List of Abbreviations

2-CysPrx: 2-cysteine peroxiredoxin

αHL: alpha hemolysin

Ag/AgCl: silver/silver chloride

BSA: bovine serum albumin

CW DPSS: continuous wave diode pumped solid state

DNA: deoxyribonucleic acid

DPhyPC: 1,2-diphytanoyl-sn-glycero-3-phosphocholine

dsDNA: double-stranded deoxyribonucleic acid

dsRNA: double-stranded ribonucleic acid

IR: infrared

KCl: potassium chloride

LCST: lower critical solution temperature

MBP: methyl binding protein

MspA: *mycobacterial smegmatis* porin A

NA: numerical aperture

OmpG: outer membrane protein G

PA: polyacrylamide

PCR: polymerase chain reaction

PEG-DMA: poly(ethylene glycol) dimethylacrylate

PNIPA: poly(N-isopropylacrylamide)

PS: polystyrene

QPD: quadrant photodiode

RecA: recombinant protein A

RNA: ribonucleic acid

ssDNA: single-stranded deoxyribonucleic acid

ssRNA: single-stranded ribonucleic acid

TRIS: tris(hydroxymethyl)aminomethane

UV: ultraviolet

Abstract

Nanopore-based resistive pulse sensing represents an important class of single-molecule measurements. It provides information about many molecules of interest (i.e. DNA, proteins, peptides, clusters, polymers, etc.) without the need for labeling. Two experiments that are especially well suited for studying with nanopore sensors are DNA sequencing and DNA-protein force measurements. This thesis will describe progress that has been made in both areas.

DNA sequencing has become an active area of research for stochastic single-molecule sensing, with many researchers striving for the ultimate goal of single-molecule *de novo* DNA sequencing. One intriguing method towards that goal involves the use of a DNA exonuclease or polymerase enzyme, which when attached close to the mouth of a pore, leads to cleavage of individual DNA nucleotide bases for loading into the pore for sensing. Though this method seems promising, the end goal has been elusive because the nucleotide motion is dominated by diffusion over the relevant length scales. This limits the likelihood of the cleaved nucleotide entering the pore to be characterized. The first part of this thesis will describe a method for addressing this problem, where it is shown that increasing the nucleotide capture probability can be achieved by lowering the bulk diffusion coefficient relative to the pore diffusion coefficient.

The second part of this thesis will describe the design and implementation of a new type of sensor that combines a biological nanopore experimental apparatus with optical tweezers. The goal of this apparatus is to develop a means to independently measure the force on a charged molecule inside of the pore. The setup will be thoroughly described, and preliminary results showing that it is possible to optically trap a micron sized bead within a few microns of an isolated biological nanopore while simultaneously making current measurements through that pore will be presented. This will enable force measurements on DNA molecules tethered to the

bead, which opens the door for the study of molecular force interactions between DNA and biological nanopores, DNA-bound protein interactions that cause diseased states, and controlled translocation of DNA through biological nanopores.

Chapter 1

Introduction

1.1 Introduction to Nanopore Sensing

Resistive pulse nanopore sensing came into view almost two decades ago when Kasianowicz et al. first used the α-hemolysin (αHL) protein, a transmembrane ion channel from *Staphylococcus aureus*, to detect the translocation of individual, single-stranded RNA (ssRNA) and DNA (ssDNA) molecules.[1,2] With this discovery, many researchers jumped into the field of nanopore-based sensors, trying to be the first to rapidly sequence DNA at the single-molecule level. Though much progress has been made on that front, the real power of nanopores lies in their ability to make measurements in a volume comparable to the size of the analyte molecules under study.[2] Being able to make these single-molecule measurements allows researchers to draw conclusions about the distribution of properties within an ensemble, rather than obtaining more generalized results based upon macromolecular sample properties.

In practice, the nanopore and membrane, whether synthetic or biological, are immersed in an electrolyte solution, so that when a potential difference is applied across the pore a measurable ionic current is developed (Figure 1). Single-molecules are then driven through the pore causing temporary blockades in the open pore current.[3] The simplicity of this setup allows for label free, *in situ* analysis of many types of molecules. For instance, nanopores have been used to analyze proteins,[4] peptides,[5] amino acids,[6] organic molecules,[7] microRNAs,[8] nerve agents,[9] explosives,[10] metal ions,[11] covalent reactions,[12] polymers,[3] biomolecular complexes,[3] and of course, DNA.[1] Some of the properties that can be extracted from the molecules being interrogated include their size distribution and charge density.[13] Initial nanopore studies involved

simple biological protein pores, however, the field has expanded to include synthetic nanopores fabricated from metal-organic[14] or inorganic materials,[13] as well as modified biological pores.[6,7,9,10,15]

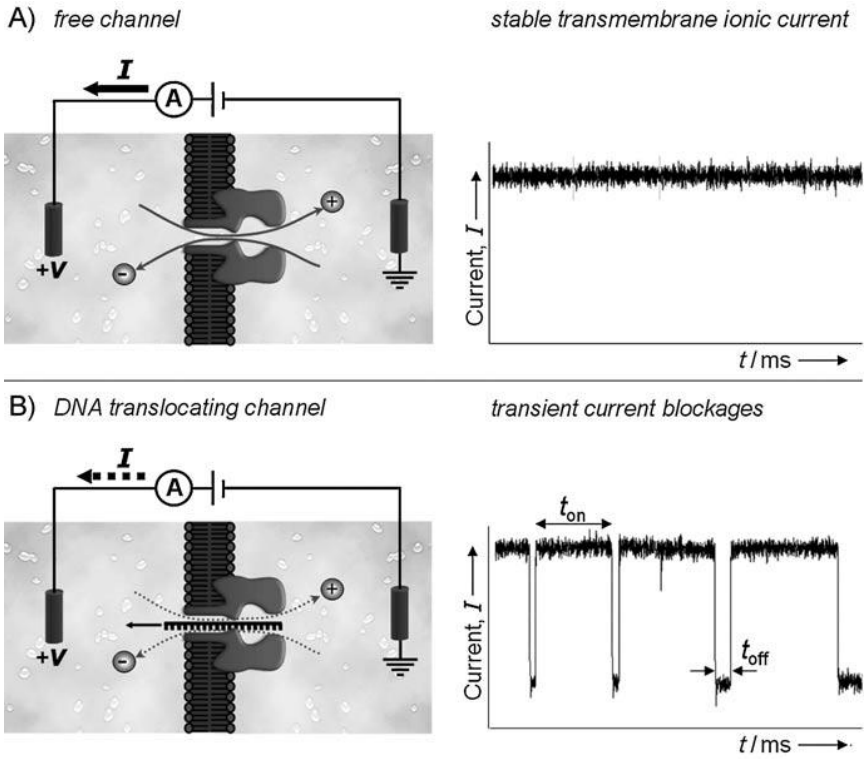

Figure 1: Representation of a typical biological nanopore experimental apparatus, with αHL embedded in a suspended lipid bilayer. (A) A stable ionic current *I* is developed when a potential difference *V* is applied across the membrane. (B) Introduction of analyte species causes transient current blockades, which can be characterized by the dwell time t_{off} and the duration between events t_{on}. Reproduced from Reference 30 with permission of John Wiley & Sons Inc.

1.1.1 Analysis with Nanopores

Nanopore sensing was developed out of a combination of Coulter-counting[16] and single-channel current recording using biological channels that respond to external stimuli.[17,18] The former is a technique used to detect microscale analytes. In Coulter-counting, a small aperture is used to connect two electrolyte filled chambers, across which a voltage is applied. This results in a measurable ionic current that is modulated by passage of analyte species. By partially blocking the aperture, the resistance of the membrane is altered. The frequency and magnitude of the

blockade events can be used to determine the concentration and size of the species respectively.[19,20] The jump to nanoscale analytics is therefore conceivable by reducing the aperture of the Coulter-counting device down to a few nanometers.

The other technique from which nanopore analysis developed, single-channel current recording, involves measuring the current through transmembrane ion channels.[17,18,21,22] These ion channels are biological proteins which control the passage of specific ions from one side of the cell membrane to the other in response to external stimuli.[23-25] Many of these channels operate via conformational changes in the protein itself. Measuring current changes in ion channels allows for detection of a specific analyte that binds to the protein and causes these conformational changes.[19,26,27] Nanopore experiments differ from single-channel current recordings in that they measure current changes caused by electrostatic or steric effects of the analyte, not conformational changes of the channel. In addition, biological nanopores typically lack the ability to bind specific analytes. In a sense they are blank and can be used for a wide variety of molecular species. Biological nanopores can also be genetically engineered to bind particular molecules,[7,9,10,12] which is different from the normal sensing mode where molecules passively drift through the pore.

1.1.2 Sensing with Biological Nanopores

Biological nanopores have the advantage of allowing consistently reproducible experiments. Their structure is determined by their amino acid sequence and, therefore, is the exact same from experiment to experiment. One of the most widely used biological nanopores is αHL from *Staphylococcus aureus*.[3,4,8,28-32] The widespread use of αHL can be attributed to its remarkable stability for a biological nanopore, along with the fact that it does not undergo

conformational changes. Thus, it provides a constant current level through which analyte blockades can be detected. In unmodified form, αHL is nonspecific and lacks the ability to bind analytes. It is composed of seven identical polypeptides that self-assemble to create a 14 stranded β-barrel structure when it comes into contact with a lipid bilayer membrane (Figure 2).[2] There is a mushroom shaped cap on the *cis*-side, above the β-barrel, with an entrance size around 2.9 nm, a 1.3 nm constriction in the middle of the protein, and a 2 nm opening on the *trans*-side.[3] The αHL protein can be chemically or genetically engineered to incorporate analyte specificity as well.[6,7,9,10,15]

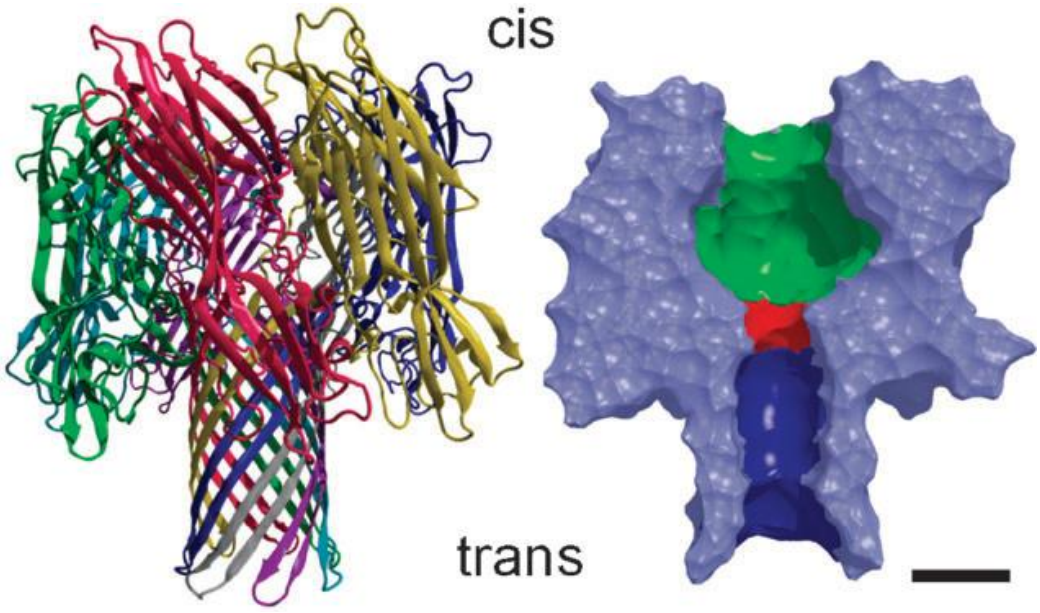

Figure 2: Structure of the αHL protein. The αHL nanopore consists of seven identical monomer units which self-assemble to form a β-barrel structure that spans the lipid bilayer membrane (left). A cross sectional view shows the inner cavity of the pore in green, the constriction in red, and the β-barrel in blue (right). The scale bar is 2 nm. Reproduced from Reference 3 with permission of The Royal Society of Chemistry.

Though much of the pioneering work done on single-molecule DNA sequencing studies evolved around αHL,[1,2,3] MspA, another proteinaceous pore studied in this thesis, has recently emerged as an alternative for biological single-molecule analysis.[33-38] MspA is also highly stable and consists of eight monomer units that self-assemble to form a bilayer spanning channel.[34] The

constriction zone is approximately 1.2 nm in diameter and contains negatively charged amino acids that facilitate the stable binding of various analytes (Figure 3).[34,35] Engineered forms of MspA have been shown to have the ability to distinguish between the current blockades of all four DNA nucleotides when the single-stranded portion of a DNA molecule is slowed by a double-stranded portion that blocks the pore restriction.[35] Taking the ability to slow down the translocation of ssDNA through MspA even further, phi29 DNA polymerase and NeutrAvidin have been employed to feed the single-stranded portion of a DNA molecule base by base through the nanopore for greater resolution of the current blockades.[36,37,38] In addition to being able to distinguish between the four basic nucleotides, MspA has the capability of mapping out epigenetic mutations that occur when certain bases are methylated.[36] Other protein pores that have also been used for sensing include: outer membrane protein G (OmpG), gramicidin, alamethicin, melittin, aerolysin, anthrax toxin, and diphtheria toxin.[33]

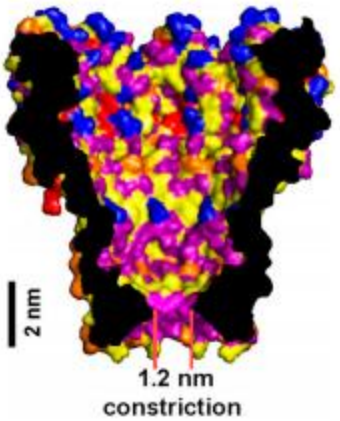

Figure 3: Crystal structure of M1MspA revealing the different classes of amino acids that make up the pore. The space-filling model shows positively charged amino acids in red, negatively charged amino acids in blue, polar amino acids in pink, hydrophobic-aliphatic amino acids in yellow, and hydrophobic-aromatic amino acids in orange. There is a small 1.2 nm constriction on the *trans*-side of the pore. Reproduced from Reference 35 with permission from National Academy of Sciences, U.S.A.

A potential drawback of biological nanopores is that they must be inserted in a quasi-controlled fashion into a lipid bilayer membrane. The bilayer may be supported on a solid

substrate, a liposome, a droplet interface bilayer, or more traditionally, on a 50-150 μm diameter orifice in a hydrophobic membrane.[3,33] After formation of the bilayer, a protein mixture is added to the experimental chamber which eventually causes spontaneous, random insertion of the proteins into the membrane. A single channel can be "captured" by patching onto the membrane with a micropipette. Other methods to obtain single channels for current recordings include flushing out the excess protein once a single insertion has been achieved or manually contacting the membrane with a glass tip that has been coated with the biological pores.

The bilayer that supports these pores is also a source of instability and may break upon pressure fluctuations, mechanical vibrations, or build up of electric charge. It is possible to reduce the chance of membrane rupture by decreasing the size of the membrane or using phospholipids that can be chemically cross-linked.[3] Additionally, the membrane may be supported by hydrogels[39] or agarose gel[40,41] to help impart stability. If done correctly, it is possible to take measurements on a single pore for multiple hours, even without added membrane support. Despite the drawbacks, biological nanopores have a specific geometry, known chemical structure, and are highly useful for reproducible single-molecule characterization. Compared to other single-molecule detection techniques, the setup is relatively simple.

1.2 Overview of Thesis

It is clear that the nanopore is a powerful tool in the realm of single-molecule studies, and the following pages will go on to discuss various techniques and analyses that biological nanopores are capable of. From potential DNA sequencing experiments,[1,15] to single-molecule mass spectrometry,[42] to combining nanopores with optical techniques,[13,43-49] the possibilities for

nanopore analysis have grown tremendously in the past couple of decades. The second chapter of this thesis will take a look at an interesting way to improve the capture rate of analyte molecules to a nanopore. This could have possible implications in single-molecule nanopore sequencing experiments. The third chapter describes an experimental apparatus that combines a biological nanopore with optical tweezers, the first known setup of its kind, and goes on to discuss calibration, current blockade, and force measurement experiments.

1.2.1 Towards Cleavage-Based Sequencing of DNA with αHL

Chapter two describes a novel way of improving the sequencing abilities of a cleavage-based nanopore sequencing engine. Initially, nanopore sensing was purported to become an easy way to sequence individual DNA strands one base at a time without the need for lengthy amplification techniques.[1,50-59] However, that goal has yet to be realized due to problems with the nanopore sensing methods used.[60] Most techniques involve feeding a single DNA molecule into the pore, but this sensing procedure does not have the single-base resolution necessary to accurately determine the sequence of bases from a single strand (i.e. the sensing regions of αHL and MspA are 12 bases[61] and 4 bases[62] in length, respectively). In addition, there have been problems with controlling the rate of translocation through the pore,[63-68] transverse field effects,[69] and membrane fluctuations.[70] A recent publication by Clarke et al. described a new way to approach DNA sequencing with the αHL nanopore that circumvents these problems.[71] In particular, their experimental setup involved an exonuclease enzyme placed near the pore mouth of an engineered αHL nanopore with a β-cyclodextrin molecule covalently attached to the pore constriction. This setup facilitated cleavage of ssDNA analyte into its constituent nucleotides, which could then be fed one-by-one into the nanopore sensor. The capture of the individual

nucleotides by the adapter revealed distinct current blockade peaks that could be resolved, thus, suggesting a feasible route to sequencing DNA with only one strand.[71]

After their work, however, a paper by Reiner et al. was published that described a potential problem with the cleavage-based nanopore sequencing engine.[32] Analytical theory and computer simulations suggested that the proposed sequencing engine would be limited by diffusion of bases away from the nanopore entrance. The probability of nucleotide capture does not begin to approach 100% until well over 500 mV, beyond the realm in which biological nanopores can be used. These problems limit the likelihood that the cleavage-based DNA sequencing engines will become useful for large scale sequencing experiments.[32]

In this thesis, chapter two will describe a possible way to remedy the inherent diffusion problem with the cleavage-based nanopore sequencing engine. Specifically, it is proposed to utilize a crowded environment directly outside of the pore that lowers the diffusion coefficient in the bulk electrolyte, while leaving the diffusion coefficient inside of the pore unaffected. It will be shown that this arrangement increases the probability to capture an analyte molecule released at the mouth of the pore. When combined with voltage driven electrophoresis, this step function diffusion technique may ultimately give the cleavage-based nanopore sequencer a better chance at accurately determining the sequence of a ssDNA molecule.

1.2.2 Optical Tweezers for Biological Nanopore Measurements

Researchers have combined optical tweezers with solid state nanopores in order to measure interaction forces with the pores, hydrodynamic slip forces, and translocation dynamics of protein/DNA complexes.[13,43-49] However, the wealth of information that can be gained by combining optical tweezers with nanopore sensing has yet to be extended to biological

nanopores. Chapter three describes the construction of a new apparatus that extends this optical tweezers/nanopore approach to biological nanopores suspended in a lipid bilayer. In addition, the experimental arrangement described has the capability of making single-molecule force measurements. This opens up the possibility of measuring the interaction force of analyte molecules with biological nanopores. A detailed description of the experimental apparatus and further research opportunities with it are discussed in this chapter.

Chapter 2

Increasing Probability to Capture via Diffusion Gradients

2.1 Introduction and Literature Review

Of the various analyte molecules studied with nanopores, DNA is perhaps of the most interest. It has been suggested that DNA might be sequenced by threading it through a single nanopore and using the change in ionic current to determine the order of the bases.[1] This would allow for rapid, label-free detection and eliminate the need for expensive and time consuming sequencing methods that need polymerase chain reaction (PCR) amplification.[50-59] The first nanopore research that suggested the potential of fast and easy DNA sequencing was performed by Kasianowicz et al. at the National Institute of Science and Technology.[1] They used an αHL nanopore embedded in a lipid bilayer membrane that was suspended between two electrolyte chambers for their experiments. By applying a transmembrane potential, polyanionic ssRNA and ssDNA in the *cis*-chamber were driven through the nanopore into the *trans*-chamber. Current blockade data was converted into a histogram of blockade lifetimes, which showed three distinct peaks (Figure 4). This was believed to indicate that the decreases in ionic current as the polymers passed through the pore were proportional to polymer length, with the longer polynucleotides spending more time in the pore lumen. To confirm that the ssDNA was translocating, and not just entering and exiting the pore from the *cis*-side, PCR amplification was performed on the electrolyte solution on the *trans*-side of the membrane after the blockade experiments. The amplification steps showed the presence of DNA on the *trans*-side, and the number of DNA molecules in that chamber was also shown to be proportional to the number of current blockades during the experiment.[1]

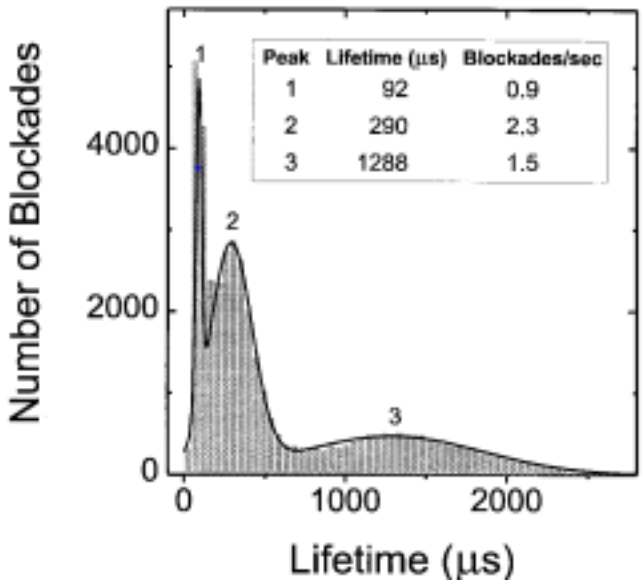

Figure 4: A current blockade histogram showing the distinct lifetimes of different length poly-U oligonucleotides. To determine the mean lifetimes a sum of three Gaussian functions was used. Reproduced from Reference 1. Copyright 1996 National Academy of Sciences, U.S.A.

Unfortunately, being able to thread a single DNA molecule through a nanopore and determine its base sequence has been quite challenging.[72] The physics of polymer translocation and lack of control of the translocation rate through a nanopore have created barriers to accurate sequencing.[63-68] However, as a step towards that sequencing goal, Clarke et al. engineered an αHL nanopore with a molecular adapter inside of the pore lumen and placed exonuclease proteins on the *cis*-side of the membrane (Figure 5).[71] The exonuclease enzyme cleaves ssDNA molecules into their constituent bases. The hope was that, with further refinement, the cleaved bases from a single exonuclease enzyme could be fed in order through the covalently attached β-cyclodextrin molecular adapter in the nanopore. The molecular adapter serves to increase the resolution of the current measurements such that each base gives rise to a distinct peak in the current blockade histogram. It was found that the nucleotides also displayed different mean dwell times, allowing for an alternative identification of bases when analyzing current traces. Under optimal recording conditions, they were able to discriminate between the four bases with 99%

confidence when only reading raw bases (i.e. ones not cleaved by the exonuclease enzyme). It was suggested that, with further experimentation involving covalently attaching the exonuclease protein to αHL and multiplexing the system, cheap nanopore sequencing of DNA could become a reality.[71]

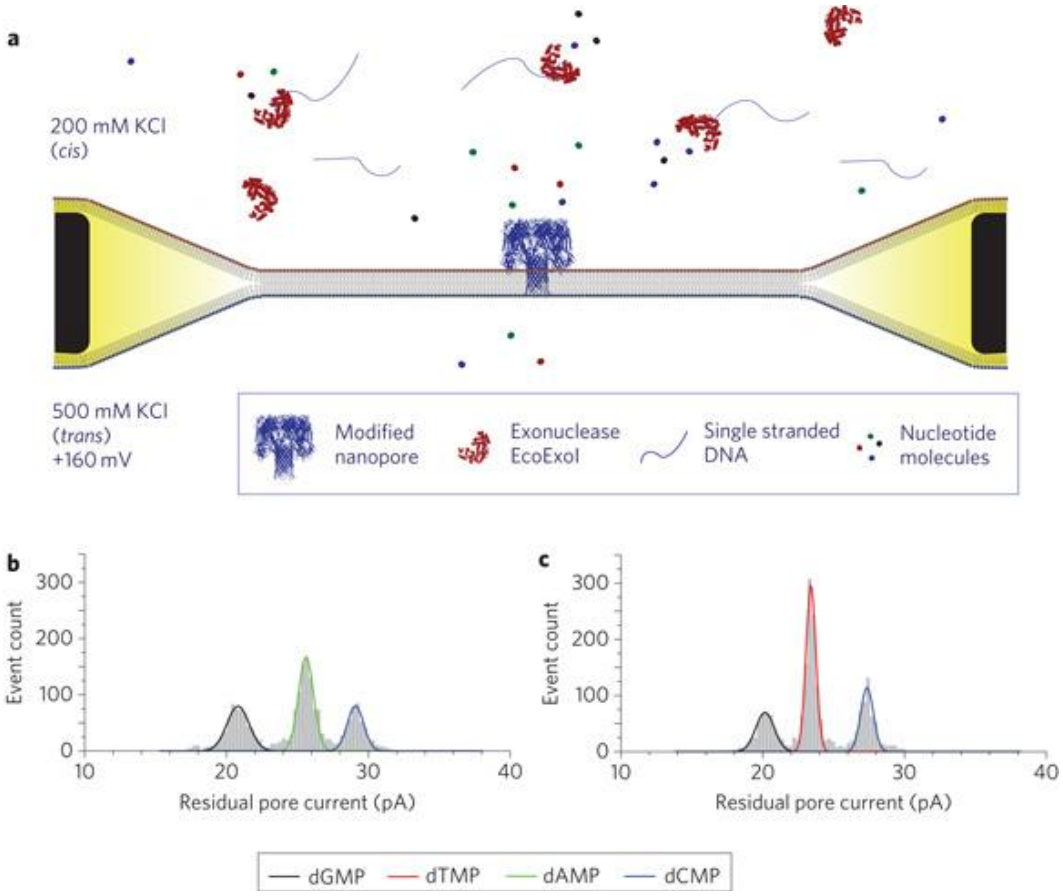

Figure 5: Experimental setup for exonuclease/nanopore based sequencing. (A) Exonuclease proteins reside on the *cis*-side of the pore where they cleave ssDNA molecules into their constituent bases. (B) Residual pore current histogram for G, A, and C bases showing the ability to resolve between them. (C) Residual pore current histogram for G, T, and C bases. Reprinted by permission from Macmillan Publishers Ltd: Nature, Reference 71, copyright 2009.

After the work by Clarke et al.,[71] a paper was published by Reiner et al.,[32] which went on to estimate that the cleavage-based nanopore sequencing engine may be limited to reading less than 80 bases accurately from an ensemble of DNA molecules, due to the diffusion of cleaved nucleotides away from the pore mouth. By fitting the residual pore current histograms from

Clarke et al. with Voigt functions instead of Gaussian functions, it was determined that the actual accuracy of the pore to discriminate between the four aforementioned bases was likely 92%, rather than the 99% initially reported. The capture probability for small diffusive particles near the entrance of the nanopore was modeled, and it was shown that in order to achieve near 100% capture efficiency with electrophoretic effects alone, transmembrane voltages of over 500 mV need to be applied. Of course, the lipid bilayer membrane is not likely to survive such high applied potentials. In addition, by increasing the potential, the mean residence time that each base spends on the β-cyclodextrin adapter would decrease, reducing the ability to distinguish between bases accurately. By increasing the bandwidth it is possible to read shorter lived events, but Reiner et al. went on to show that the maximum detection probability, combining bandwidth and voltage effects, was limited to ≈ 75% (Figure 6). In the Clarke et al. paper, only about 30 events per second were observed with a mononucleotide concentration of 40 μM, much less than the calculated interaction rate of 30,000 events per second estimated by Reiner et al. That corresponds to only about 1 in 1000 events being observed by the β-cyclodextrin adapter, suggesting many events were too short-lived to be detected. It was estimated that only about 85 bases of a 100 base pair DNA sequence could be accurately determined by reading 200 identical sequences with this cleavage-based nanopore sequencing engine, which would severely limit its applicability in single-molecule sequencing experiments.[32]

Though the Clarke et al. system has its merits, it is obvious that some issues need to be addressed before being able to accurately sequence even moderate length DNA strands. One of the biggest problems of the system is that of diffusion. Reiner et al. estimated that the probability of capturing a given base was roughly 75%.[32] An easy way to amend this problem would be to attempt to decrease the possibility of diffusion away from the pore mouth. This thesis chapter

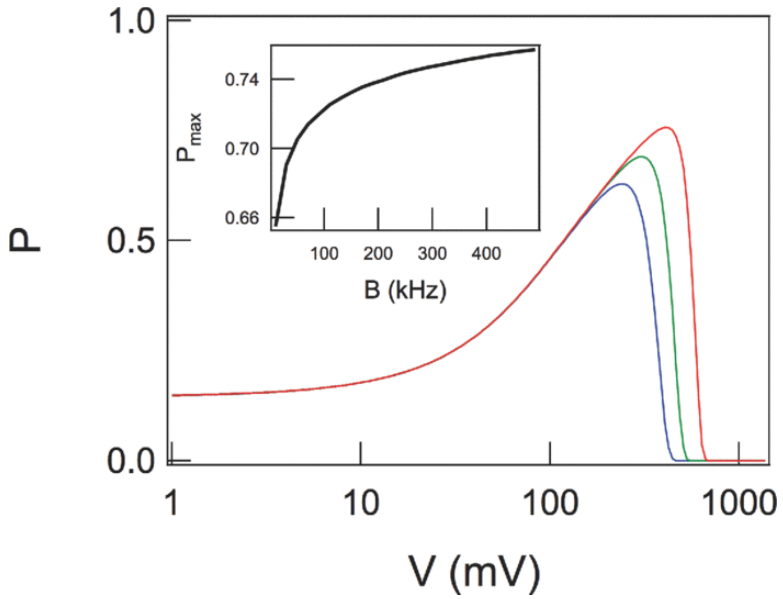

Figure 6: Bandwidth and applied potential effects on the probability of reading an individual ssDNA base correctly. Increasing the applied potential can help to increase the capture probability, but at the same time it will decrease the residence time of a base inside the molecular adapter in the pore. Increasing the bandwidth allows for faster measurements, thus, a higher potential can be used in experiments. However, the inset figure shows that the capture probability reaches a plateau of roughly 0.75 as bandwidth is increased. Increasing the bandwidth also increases the noise, which could cause problems when trying to resolve different current blockades. Reprinted with permission from Reference 32. Copyright 2012, AIP Publishing LLC.

will address an interesting method to increase the capture probability for small, diffusing DNA mononucleotides. The idea involves using a crowded environment directly outside of the nanopore mouth on the side with the nucleotide cleaving enzyme, akin to the crowded environments in cells that tend to increase the recapture rate between analyte molecules and their targets.[73,74] The crowded environment is modeled as change in the bulk diffusion coefficient D_{bulk} that, when decreased relative to the pore diffusion coefficient D_{pore}, increases the probability a given base will be captured and read. Random walk simulations are implemented to show the change in capture probability with D_{bulk}/D_{pore}. Strategies to optimize this effect and to implement it experimentally are also discussed.

2.2 Methodology

2.2.1 Random Walk Simulations

All random walk simulations are performed in MATLAB following a previously described protocol.[32] The nanopore environment is simulated using a three dimensional diffusion model with voltage bias. The nanopore is modeled as a cylinder with a length L_{pore} of 10 nm and radius R of 1.2 nm. Nucleotides are initially positioned at $r = 0$ and $z = L$, which is 6 nm above the capture plane in the pore located at the origin, to simulate the position of the cleaving protein (Figure 7).

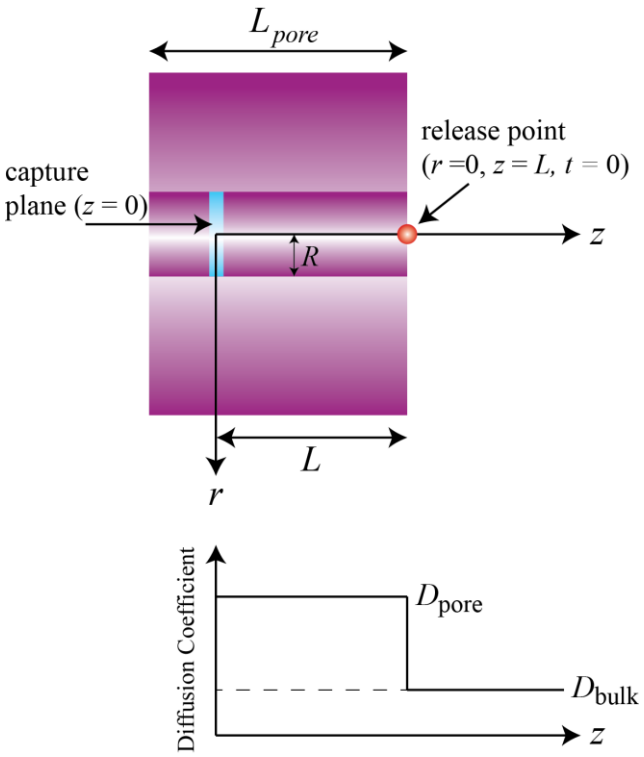

Figure 7: Model of the nanopore sensing apparatus with a step function diffusion coefficient. (Top) The DNA nucleotides are modeled as point particles released at time $t = 0$ centered at the pore mouth a distance L away from the capture plane (blue). The pore has radius R and length L_{pore}. Once released, the particle takes a random walk and is either captured if it contacts the capture plane, or escapes into the bulk electrolyte solution on the right side of the pore. (Bottom) To increase the probability of capture, the diffusion coefficient of the medium is adjusted using a step function diffusion coefficient. Specifically, the diffusion coefficient of the bulk is reduced from that of the pore to simulate a crowded environment, much like in biological cells.

Nucleotides are released and a uniformly distributed random number is chosen to determine which cardinal direction (*x*, *y*, or *z*) to move for the initial step, while the step length is determined by generating a Gaussian distributed random number with zero mean and a standard deviation of $(6D\Delta t)^{1/2}$. The time duration of these random steps is held constant with $\Delta t = 1$ ps. If the nucleotide resides outside of the pore, then voltage effects are neglected and another Gaussian distributed number is generated to determine the next step. If the nucleotide resides inside of the pore, its next step will have a drift term contribution ($v_d \Delta t$) that drives the nucleotide to the capture plane near the bottom of the pore. If the nucleotide hits the pore wall ($r_{old} < R, r_{new} > R \; and \; L > z_{new} > 0$) or the membrane ($r_{new} > R, z_{old} > L$ and $z_{new} < L$), it is bounced back to its original location and a new step is calculated. This treatment of reflections off of the simulation boundaries has been shown to be accurate to $O(\Delta t)$.[75] The diffusion coefficient used to calculate step length is either $D = D_{bulk}$ or D_{pore}, depending on where the particle is located before the step, where D_{bulk} and D_{pore} represent the nucleotide diffusion coefficient in the medium outside and inside of the pore respectively. The simulation is ended if the nucleotide reaches the capture plane of the pore (i.e. it was captured) or after a 1 μs cutoff (i.e. it was not captured). Time to capture is noted if the nucleotide is captured.

In the random walk simulations, there is a step function change in the diffusion coefficient between the pore and the bulk medium which must be taken into account. This necessitates that the step size must change as the particles cross the interface at $z = L$, due to the change in diffusion coefficient. If the particle moves from the bulk electrolyte solution with a lower diffusion coefficient, to pore region with a higher diffusion coefficient, the step length is rescaled by using $\Delta z_{pore,corrected}/\Delta z_{pore,uncorrected} = (D_{pore}/D_{bulk})^{1/2}$.[76] This corrective measure ignores the fact that there is also a step function change in the drift velocity crossing the

boundary, but is justified for small time steps since the diffusion length scales as $(\Delta t)^{1/2}$, while the drift length scales as Δt. When the particle crosses from the pore region to the bulk region, a similar corrective factor is applied, however, it is also necessary to calculate the probability that the particle will reflect back off the interface at $z = L$ when crossing into a region with a lower diffusion coefficient.[76] To do this, a random number from a uniform distribution is chosen and compared to the probability of reflection $P_r = (D_{pore}/D_{bulk})^{1/2}$. The particle is returned to its original position if the random number selected is greater than P_r. If the random number selected is less than or equal to P_r, the particle is moved through the interface with the portion of the step calculated in the bulk such that $\Delta z_{bulk,corrected}/\Delta z_{bulk,uncorrected} = (D_{bulk}/D_{pore})^{1/2}$.[76,77]

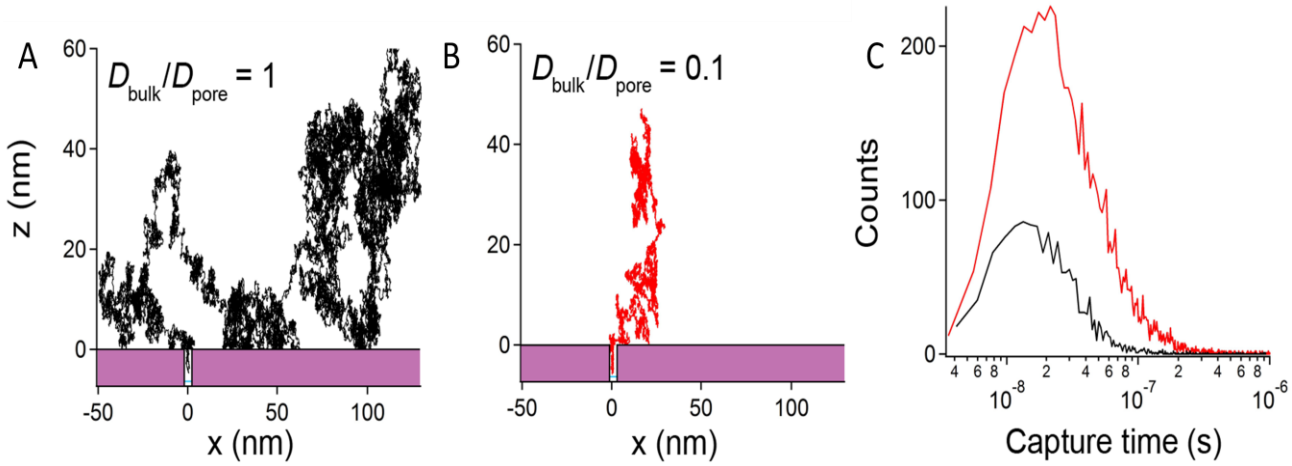

Figure 8: Planar projections of random walk simulations for different diffusion coefficient ratios with corresponding capture time distributions. For the projections, the particles are released at $r = 0, z = L$ and undergo a 10 μs random walk simulation. (A) Matching diffusion coefficients allow the particle to migrate over a large volume. (B) When the diffusion coefficient of the bulk is reduced by 90%, it can be seen that the particle now migrates over a much smaller volume. (C) Capture time distributions ($D_{bulk}/D_{pore} = 1$, black; $D_{bulk}/D_{pore} = 0.1$, red) show the probability of capturing a particle asymptotically approaching zero for times over 500 ns. The larger area under the red curve indicates a better capture efficiency for the case where $D_{bulk}/D_{pore} = 0.1$. The parameters used for the trajectories are: L_{pore} = 10 nm, L = 6 nm, R = 1.2 nm, D_{pore} = 3×10^{-10} m^2/s,[32] and V = 0.

The random walk steps of a single particle are shown as an *x*-*z* planar projection in Figure 8. The distribution of the capture times is shown for cases with and without a step decrease in the diffusion coefficient. It can be seen that the capture probability is asymptotically approaching zero after 500 ns, justifying the 1 μs cutoff used in the simulations.

2.3 Results and Discussion

2.3.1 Results

The diffusion-step model system is illustrated in Figure 7. The nanopore is modeled as a right circular cylinder oriented about the *z*-axis with the nucleotide cleaving enzyme centered at the pore entrance. The membrane that the pore is embedded in is assumed to be perfectly reflecting at the points $z = L, r > R$, where L is the distance from the entrance of the pore to the capture plane and R is the pore radius. To model the crowded environment in the bulk solution, the diffusion coefficient is described by a step function, with the diffusion coefficient of mononucleotides in the bulk being smaller than that in the pore. The pore length L_{pore} is different from the distance to the capture plane L.

To simplify matters, any nucleotide that reaches the capture plane is assumed to be captured and read with 100% efficiency, however, it is likely that this will not be the case in an actual experiment. The capture plane is localized at $z = 0$ and particles are released in the center of the pore at $r = 0$ and $z = L$ at time $t = 0$. Thus, the initial concentration profile for each cleaved particle can be represented by a delta function:

$$C(r = 0, z = L, t = 0) = 2\pi\delta(r)\delta(z - L)/r. \quad (1)$$

An approximate solution for the capture probability given the above concentration profile has already been found.[32] The time-integral of the flux rate of mononucleotides to the capture plane gives the probability that a nucleotide will be captured P_{cap} (assuming 100% efficiency):

$$P_{cap} = -\int_0^{\infty} D_{pore} \frac{\partial C}{\partial z}\Big|_{z=0} dt \tag{2}$$

where D_{pore} is the diffusion coefficient within the nanopore and C is the concentration profile, which is a solution of the Fokker-Planck equation:

$$\nabla \cdot (D\nabla C) - \boldsymbol{v_d} \cdot \nabla C = \frac{\partial C}{\partial t} \tag{3}$$

where v_d is drift velocity of the nucleotide in the pore $v_d = \mu V / L_{pore}$, V is the applied membrane voltage, μ is the electrophoretic mobility, L_{pore} is the length of the pore and D is the diffusion coefficient, which is not constant in this case. The boundary conditions are:

$$\begin{aligned} C(z = 0, t) &= 0 \text{ Absorption at the capture plane} \\ \frac{\partial C}{\partial r}\Big|_{r=R, 0<z<L} &= 0 \text{ Reflections off the interior pore wall} \\ \frac{\partial C}{\partial z}\Big|_{r>R, z=L} &= 0 \text{ Reflections off the membrane.} \end{aligned} \tag{4}$$

Though there is no known closed-form solution to Equation 3 with the boundary conditions given in Equation 4, an approximate solution can be obtained from the assumptions that the pore radius is small compared to the length of the pore ($R \ll L_{pore}$), so the pore can be modeled as a

one-dimensional line, and the coupling of the pore to the bulk can be described with a radiating boundary condition:[78,79]

$$\kappa C(L,t) = -D_{pore}\left.\frac{\partial C}{\partial z}\right|_{z=L} + v_d C(L,t) \tag{5}$$

where $\kappa = 4D_{bulk}/\pi R$. Using these assumptions, an expression for nucleotide capture probability has already been derived:[32]

$$P_{cap}\left(V, D_{bulk}/D_{pore}\right) = \frac{\exp\left(\frac{\alpha}{2}\right)}{\cosh\left(\frac{\alpha}{2}\right) + \left(1 + \frac{2\beta D_{bulk}}{\alpha D_{pore}}\right)\sinh\left(\frac{\alpha}{2}\right)} \tag{6}$$

where the explicit expressions for the model parameters α and β are:

$$\alpha = \frac{|v_d|L}{D_{pore}} \tag{7}$$

$$\beta = \left(\frac{4L}{\pi R}\right) \tag{8}$$

where D_{bulk} is the nucleotide diffusion coefficient in the electrolyte solution on the *cis*-side of the pore, D_{pore} is the nucleotide diffusion coefficient inside of the pore ($z < L$), R is the radius of the pore, v_d is the drift velocity, and L is the distance from the capture plane to the pore mouth.

It was assumed before that $D_{bulk} = D_{pore}$,[32] but now that restriction has been relaxed. The capture probability explicitly depends on the ratio of the two diffusion coefficients inside

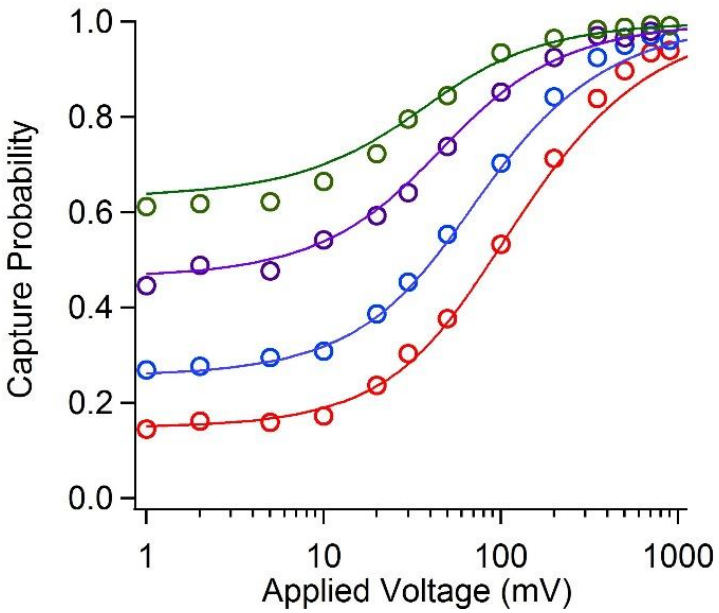

Figure 9: Capture probability versus applied voltage under various diffusion coefficient ratios calculated from random walk simulations. Each set of numerical data points is well fit with Equation 6 using appropriate values of α and β. Increasing the ratio D_{pore}/D_{bulk} increases the capture probability for a given applied voltage. This behavior is observed, for various ratios of D_{pore}/D_{bulk}. The different lines correspond to D_{pore}/D_{bulk} = 1 (red), 2 (blue), 5 (purple), and 10 (green). The parameters used in the simulations and the analytical expression are: L = 6 nm, R = 1.2 nm, L_{pore} = 10 nm, μ = 3.28 × 10^{-8} m^2/Vs, and D_{pore} = 3 × 10^{-10} m^2/s.[32]

and outside of the pore and not on either diffusion coefficient independently. The capture probability as a function of increasing potential is shown in Figure 9 for different D_{pore}/D_{bulk} values. The open points are the random walk simulation results from the model shown in Figure 7, while the solid lines are plotted using Equation 6 with the appropriate model parameters. As can be seen, there is good agreement between the analytical model and the random walk simulations without any fitting parameters. Increasing the applied transmembrane voltage increases the capture probability as previously demonstrated.[32] However, it can also be seen that the capture probability is altered by the diffusion coefficient ratio. In biological nanopore sensing systems, there are limitations to the magnitude of the applied transmembrane voltage, so the

results in Figure 9 provide further motivation for studying alterations of the bulk diffusion coefficient via inert crowding molecules.

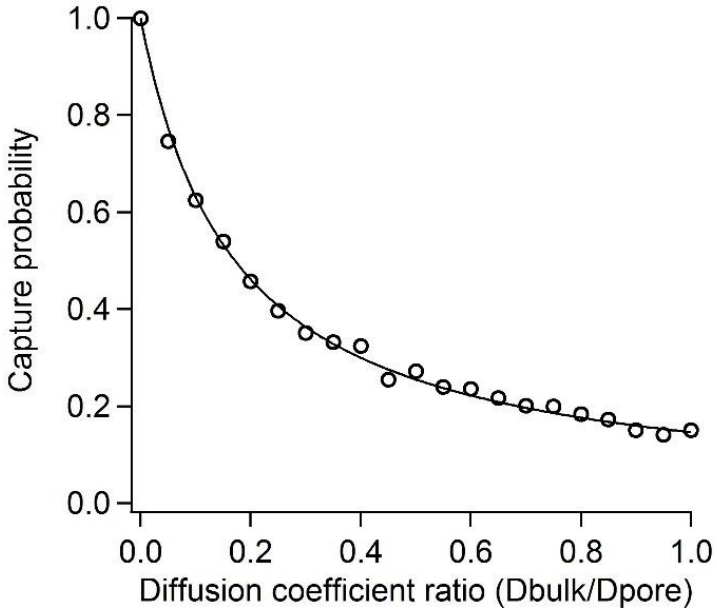

Figure 10: Capture probability versus diffusion coefficient ratio D_{bulk}/D_{pore} with no applied potential. The capture probability is seen to increase as the diffusion coefficient of the bulk decreases relative to that of the pore. The model parameters used are the same as in Figure 9.

The explicit dependence between the capture probability with no applied potential and the ratio of the two diffusion coefficients is shown in Figure 10. The solid line shows good agreement between the random walk simulations and Equation 6. It is obvious that the step decrease in the diffusion coefficient going from the inside to the outside of the pore improves the probability that a given nucleotide will be captured and read by the nanopore sensor. To determine which adjustment, voltage or diffusion, yields the best enhancement to the capture probability, consider Equation 6 in the limit of large α (i.e. high applied potentials), where $\exp(\alpha) \approx 2\cosh(\alpha) \approx 2\sinh(\alpha)$. In this limit, Equation 6 becomes:

$$P_{cap} = \frac{1}{1 + \left(\frac{4D_{pore}L_{pore}}{\pi R\mu}\right)\frac{1}{V}\frac{D_{bulk}}{D_{pore}}} \quad . \tag{9}$$

For sufficiently high voltage ($V \geq 100$ mV → $\alpha \geq 6.6$ for the parameters studied), it appears that the increase in voltage by a given factor is equivalent to reducing the diffusion coefficient by that same factor (i.e. doubling the voltage is equivalent to halving the diffusion coefficient ratio). Figure 11 shows a plot of Equation 9 with the fit parameters from Figure 9. For typical biological sensing applications, transmembrane voltages are limited to 200 mV or below. Without adjusting

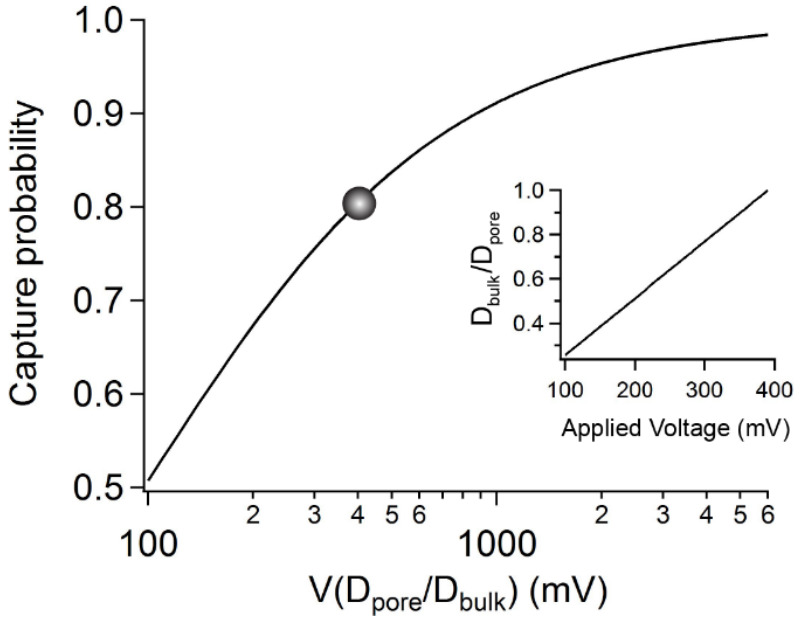

Figure 11: Relationship between changes in applied voltage and diffusion coefficient ratios, and their affect on the capture probability. At sufficiently large voltages the analytical capture probability formula reduces to Equation 9 in the text. This allows one to parameterize the capture probability in terms of the product of the diffusion coefficient ratio and the applied voltage. The model parameters used are identical to those used in Figures 9 and 10. The solid circle at 80% capture probability corresponds to VD_{pore}/D_{bulk} = 390 mV. (Inset) The voltage required to obtain 80% capture probability can be reduced by decreasing the bulk diffusion coefficient. For example, a diffusion coefficient ratio of D_{pore}/D_{bulk} = 0.4 would only require an applied voltage of 156 mV to achieve an 80% capture probability.

the diffusion coefficient at all, the maximum expected capture probability will remain below 75% even at voltages above 200 mV as described before.[32] However, by reducing the bulk diffusion coefficient, it is possible to perform the experiment with more biologically compatible voltages, thus, motivating the inclusion of a step function in the diffusion coefficient.

2.3.2 Implementation

The work above clearly shows the ability to increase the capture probability by decreasing the diffusion coefficient outside of the pore volume. There are many ways to implement this effect, and some of the most simple would involve the use of biologically compatible gels such as agarose, polyacrylamide (PA), or alginate in the *cis* electrolyte solution. Studies by Jeon et al. and Shim et al. have already demonstrated the ability to make conductance measurements on gel encapsulated lipid membranes.[39,40] The above results may suggest that the best route to ensuring 100% capture probability is to set $D_{bulk} = 0$. However, this is obviously not feasible, since it would be impossible to perform the experiments if molecules in the bulk could not diffuse towards the nanopore sensor. Also, it is necessary that the ionic conductivity remain at an acceptable level in order to make current measurements through the pore.

A simple relationship between the change in conductivity σ/σ_o and its relation to the change in the electrolyte diffusion coefficient D_{bulk}/D_{pore} is:[80]

$$\phi_w \frac{D_{bulk}}{D_{pore}} = \frac{\sigma}{\sigma_o} \tag{10}$$

where ϕ_w is the volume fraction of water. A decrease in solution conductivity will increase the access resistance to the pore. Typical, unmodified access resistances are several orders of magnitude lower than the resistance of αHL (~10 kΩ vs. ~1 GΩ). Thus, it seems likely that the diffusion coefficient ratio could be reduced significantly before problems with a high access resistance arise. For instance, a very high agarose gel fraction of 10% ($\phi_w = 0.9$) yields a reduction in the electrolye diffusion coefficient of ~0.6.[80] According to Equation 10, this would amount to a conductivity of 54% of its normal value, which would have a negligible effect on the sensing capabilities of αHL.

A study by Jeon et al. used a 7.5% (w/v) mixture of poly(ethylene glycol) dimethylacrylate (PEG-DMA) monomers and 1% Igracure in the electrolyte solution, which, when irradiated with broad spectrum UV light, formed a hydrogel around the lipid bilayer membrane.[39] By releasing αHL at the top of the gel structure, protein insertion events were observed 2-10 hours later as compared to the typical 0.5-2 hours without a gel, corresponding to a 70% decrease in the effective diffusion constant. Another study used agarose layers which were gelled *in situ* around a lipid bilayer membrane containing αHL.[40] It was shown that the agarose gel encapsulated membrane was able to retain a high membrane seal of >10GΩ for 57 hours on average, in addition to being a portable biological single-molecule sensing device.

Agarose gels have been more intensely studied do their widespread use in biological applications. The proteins lactalbumin, ovalbumin, and BSA have been thoroughly investigated in different agarose gel concentrations, and, at an agarose volume fraction of 7.3%, were shown to have their diffusion coefficients reduced to about 30% of their original values.[81] Different molecular weight samples of ficoll had reductions in diffusion coefficient ranging from 23-39% of their original values for the same gel concentration.[81] Alginate[82] and PA[83] gels were shown to

have similar reductive effects on the diffusion coefficient. Another way of altering the diffusion coefficient involves self-crowding. Increasing the volume fraction of BSA in solution to around 30% has been shown to decrease the relative diffusion coefficient of BSA by almost an order of magnitude.[84] A decrease in the diffusion coefficient of analyte in the bulk electrolyte by this amount would correspond to approximately a 90% capture probability at an applied potential of only 75 mV. This is considerably lower than the case for matching diffusion coefficients, which would require an applied potential of approximately 500 mV to achieve the same capture probability.

Though decreasing the diffusion coefficient to extremely low values may increase the capture probability, a gel concentration too high may also decrease the on-rate of ssDNA molecules to the pore so much that experiments could become inordinately long.[85] The capture rate for DNA molecules to the exonuclease protein scales linearly with D_{bulk}, so reducing this diffusion coefficient by 90% would reduce the number of DNA molecules that can be analyzed by the same amount. This may necessitate the need for a controlled adjustment of the viscosity near the pore. This could be achieved with localized heating of the nanopore area via an IR laser[86] or plasmonic excitation[87-89] that induces a lower critical solution temperature (LCST) size transition in the buffer molecules. One polymer that exhibits this behavior is poly(N-isopropylacrylamide) (PNIPA), which has an observed phase transition temperature around 32 ^{o}C.[90] Continued heating via an IR laser would keep the molecules in a compact state, and when a ssDNA molecule is captured by the exonuclease protein, the laser could be shut off, causing the polymer molecules to expand and D_{bulk} to drastically decrease. After the ssDNA molecule is cleaved and read, the laser could be turned back on and the process repeated.

2.4 Conclusions

The role of a step decrease in the diffusion coefficient going from inside of the pore to the bulk solution has been demonstrated to improve the prospects of cleavage-based nanopore sequencing. It has been shown that the decrease in bulk diffusion coefficient in the *cis*-side electrolyte will increase the capture probability of nucleotides released near the nanopore mouth. This could be achieved by the use of a crowded molecular environment, which would have a slight, but not problematic effect on the conductivity. Random walk simulations were shown to validate a simplified analytical model, and at large applied voltages ($\geq$ 100 mV) the capture probability is increased through either a reduced diffusion coefficient ratio or increased transmembrane voltage. These results suggest improved prospects for cleavage-based nanopore sequencing engines.

Chapter 3

Optical Tweezers for Biological Nanopore Measurements

3.1 Introduction and Literature Review

Nanopores have been used to characterize the unbinding of proteins from DNA molecules.[91] The applied transmembrane potential creates an electrophoretic force on the DNA strand, which in turn can be directly applied to any protein molecule bound to the DNA. This provides important information for several types of protein-DNA interactions, but it is not possible to quantify the force with this measurement unless one knows the charge on the DNA molecule. The charge cannot be independently determined from a nanopore measurement. To address this issue, one could couple the DNA to a micron sized bead and hold the bead in an optical trap. Assuming the force of the trap has been properly calibrated, it would then be possible to independently measure the force on a DNA strand versus the applied voltage, from which one could determine the charge on a DNA molecule confined in a pore. This has been demonstrated with solid state nanopores using single RNA and DNA molecules,[13,43,44] but no such measurement has ever been performed on a biological nanopore. The reason for this is simple, the biological nanopore is difficult to localize near the focus of an optical trap. This chapter describes the first demonstration of an optical trap positioned within the vicinity of a biological nanopore sensor.

Optical tweezers use a tightly focused incident laser beam, which creates a strong electric field gradient, in order to trap small dielectric objects such as polystyrene (PS) microbeads or molecules. The tweezers allow experimenters to accurately position a trapped bead within a few micrometers of the nanopore.[43,44] Ashkin first observed optical trapping of dielectric particles via

radiation pressure in the late sixties and early seventies using two oppositely directed laser beams to create an optical potential well.[92] Later on, Ashkin et al. published a paper describing a single-beam gradient force optical trap.[93] There are two opposing forces acting on particles in an optical trap, the scattering force and the gradient force. The scattering force is in the direction of the incoming light and acts to push the particle out of the optical trap. On the other hand, the gradient force is caused by the gradient of the field intensity and points towards the center of the beam waist. With a highly focused laser beam, the gradient force dominates the scattering force and is large enough to control the axial stability of the particle and hold it in the trap.[93]

For particles with an index of refraction greater than the medium in which they are suspended, that are also much larger than the wavelength of incident light λ, the Mie size regime, ray optics can be used to describe the origin of the gradient force. Rays of light from the laser are tightly focused and then refracted when they come into contact with the dielectric sphere seen in Figure 12. The change in direction of the refracted rays *A'* is due to a change in momentum of the light. There is also an equal and opposite change in momentum of the particle required by Newton's third law. The reflections R_1 and R_2 contribute to a lesser scattering force. The resultant force F_A acts to pull the particle back towards the beam focus. When the particle passes through the focus the resultant force acts in the opposite direction to push the particle back towards the focus. Thus, the gradient force acts to trap the particle in a spring-like potential well.[93]

If the particle diameter is much less than the wavelength of light, then Rayleigh scattering effects must be considered. In this case, the particle can be treated as a point dipole in a varying electromagnetic field. The Lorentz force law can be used to calculate the gradient and scattering

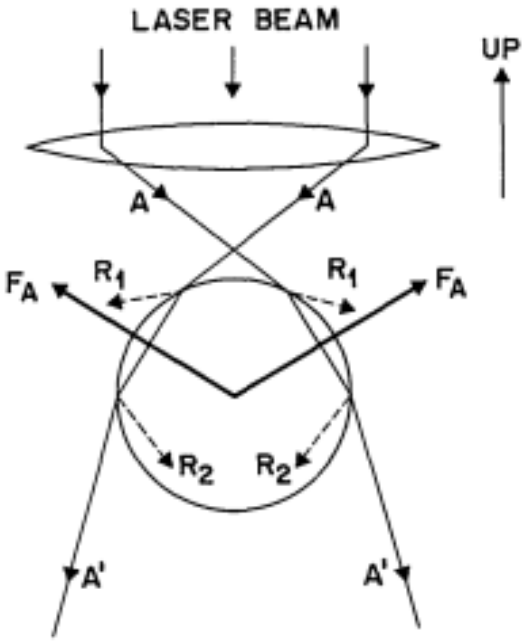

Figure 12: Ray optics diagram of a spherical Mie particle trapped in a single-beam gradient force optical trap. The laser rays *A* are focused through an objective and are refracted and reflected when they contact the dielectric particle. The rays are refracted and reflected again as they exit the dielectric particle. In the refractions and reflections, momentum is transferred from the light to the dielectric particle, resulting in a force F_A that acts to pull the particle back towards the beam focus. Adapted with permission from Reference 93.

forces acting on this point dipole. Ashkin et al. calculated the magnitude of the scattering force F_{scat} on the particle to be:

$$F_{scat} = \frac{I_0}{c}\frac{128\pi^5 r^6}{3\lambda^4}\left(\frac{m^2-1}{m^2+2}\right)n_b \tag{11}$$

where I_0 is the incident light intensity, c is the speed of light, r is the particle radius, λ is the wavelength of incident light, n_b is the dielectric constant of the medium, and m is the dielectric constant of the particle divided by the dielectric constant of the medium. For a spherical particle of polarizability α, the magnitude of the gradient force F_{grad} is:

$$F_{grad} = -\frac{n_b}{2}\alpha\nabla E^2 = -\frac{{n_b}^3 r^3}{2}\left(\frac{m^2-1}{m^2-2}\right)\nabla E^2 \,. \quad (12)$$

So, as long as the backwards axial gradient force is greater than the forward-scattering force, then particles in the Rayleigh size regime can be optically trapped.[93]

Though the first trapping of small particles by gradient force optical traps was observed decades ago,[92,93] it wasn't until 2006 that researchers combined this technique with the single-molecule sensing abilities of solid state nanopores. Keyser et al. used a PS microbead coated with λ-DNA via a streptavidin/biotin linker as the object to be trapped near a solid state nanopore.[43] After attaching the DNA to the bead, the bead was optically trapped beneath the nanopore membrane and manipulated towards the nanopore. An electric field was applied to electrophoretically force a DNA molecule into the pore, which caused an increase in ionic current through the pore while the DNA was inside (Figure 13).[43,44] During this time, the displacement of the bead in the optical trap was observed in order to determine the electrophoretic force acting on the DNA molecule. When the bead became stationary in the trap, it was assumed that the optical trapping force acting on the bead was equal and opposite to the electrophoretic force. The data obtained from these experiments allowed the researchers to extract an accurate measure of the charge per base pair of the λ-DNA (0.50 ± 0.05 e^-/bp) and the force acting on the DNA while it was in the nanopore (23 ± 2 pN/mV).[43,44]

Hout. et al. used this optical tweezers combined with a solid state nanopore approach to make direct force measurements on double-stranded RNA (dsRNA) and double-stranded DNA (dsDNA).[13] Again, streptavidin coated PS microbeads that were functionalized with biotinylated dsDNA or dsRNA were utilized. The beads were trapped and brought into close proximity with the nanopore while a transmembrane voltage was applied. The position of the bead and location

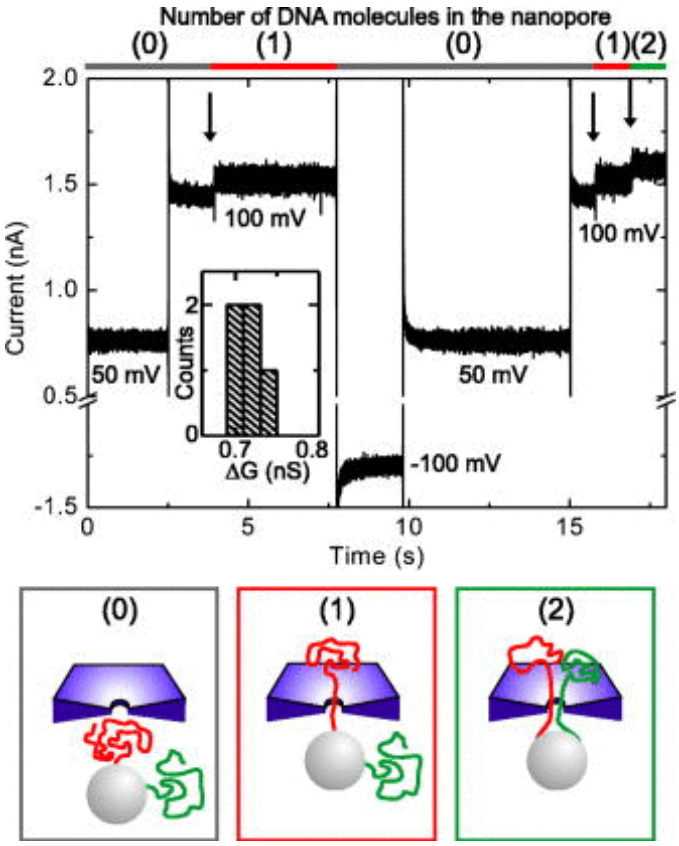

Figure 13: Current trace showing the capture of DNA strands versus time. Applied voltages are listed in the figure, with arrows marking the capture of a single DNA molecule in the nanopore, concomitant with an increased conductance. The numbers on the top of the graph give the number of DNA molecules in the pore at a given time. The inset figure shows a histogram for the conductance change as DNA molecules are captured. The pictorial representation at the bottom shows the pore with no DNA molecules, one DNA molecule, and two DNA molecules inside of it. Reprinted with permission from Reference 44. Copyright 2006, AIP Publishing LLC.

of dsDNA or dsRNA were tracked by a positioning laser and ionic current respectively. It was found that the measured electrophoretic force on the PS microbead depended linearly on the voltage for all molecules investigated (Figure 14). An interesting result was that the forces on the dsRNA and dsDNA were roughly equal within the same nanopore, with the force on dsRNA being slightly lower at $f = 0.11 \pm 0.02$ pN/mV versus $f = 0.14 \pm 0.03$ pN/mV for the dsDNA. The molecules Hout et al. looked at were significantly shorter than the λ-DNA molecules previously reported, 3.2 to 4.2 μm contour length versus 16 μm, thus, demonstrating reliable force measurements very close to the nanopore. This work extended the applicability of the

optical tweezers and nanopore setup by opening the door to look at even shorter molecules, which are typically easier to synthesize.[13]

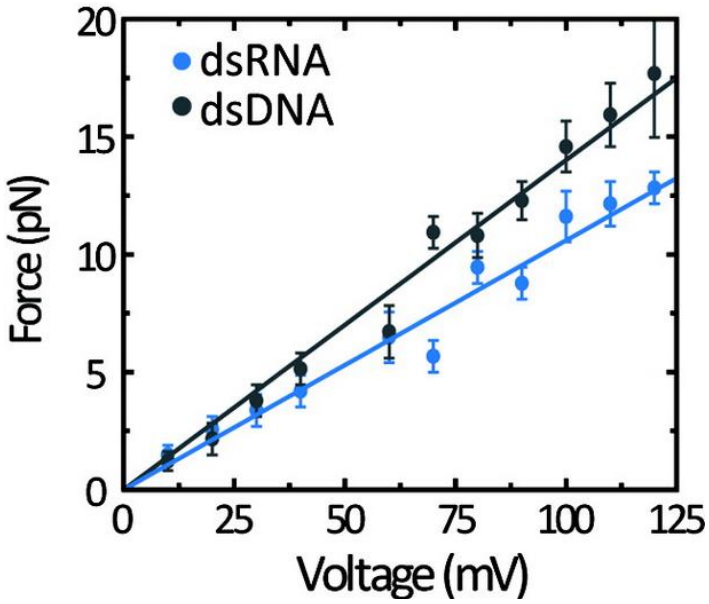

Figure 14: Dependence of the electrophoretic force on the applied potential for dsRNA and dsDNA. Data was taken using the same 22 nm pore. There is a linear relationship between the applied voltage and the measured force acting on a dsRNA and dsDNA molecule inside of the nanopore. The slopes of the trendlines give the effective force in units of pN/mV. Reprinted with permission from Reference 13. Copyright 2010 American Chemical Society.

Another group studied the translocation of ligand-complexed DNA using optical tweezers and solid state nanopores.[49] Sischka et al. looked at the binding forces between recombinant protein A (RecA) and 2-cysteine peroxiredoxin (2-CysPrx) molecules with λ-DNA. The RecA forms stable nucleoprotein filaments on the DNA, while the 2-CysPrx binds nonspecifically. Researchers were able to determine the exact location of the proteins bound to the DNA strand using a combination of quantitative 3D optical tweezers and ionic current measurements. This was accomplished by threading the protein-DNA complex into and out of the pore while monitoring ionic current, force, and *z*-distance from the pore. A small dip in the ionic current, accompanied with a change in the measured force as the DNA was moved through the pore, indicated that the protein must be passing through the nanopore. For the RecA complexed DNA,

the force jumped from a steady 7 pN to 17 pN at z = 10.1 μm, signifying the presence of a RecA-coated DNA filament at that point on the DNA strand. For the DNA-2-CysPrx complex, decreases in the effective force and current signals were observed at differing points along DNA strands. The differing effective forces are due to the fact that RecA has a negative surface charge, while 2-CysPrx has a positive surface charge. This results in increased and decreased electrophoretic forces respectively. This work demonstrated that it may be possible for easy, label-free detection of DNA-binding ligands and their locations along DNA strands.[49]

Spiering et al. went a step further to study single-molecule translocation dynamics of DNA-bound protein (Figure 15).[48] Building on the work of Sischka et al., Spiering's group found distinct, asymmetrical force signals that depended on the protein charge states, the DNA elasticity, and counterionic screening in the buffer. Using theoretical arguments, it was found that there were two metastable states corresponding to the bound protein being on either side of the membrane. This was confirmed during the experiment. As the protein approached the pore, the force equilibrium destabilized, and the protein quickly translocated through the pore to another force equilibrium, which was seen by an abrupt change in the measured force. As the protein was pulled further away, it contributed less to the force equilibrium, and the measured force relaxed to its original value for just DNA in the nanopore. It was also found that the measured force was linearly dependent on the voltage and exhibited a small hysteresis upon moving the DNA/protein constructs back and forth through the pore. Combining the theoretical work with experimental results, the charges for the two proteins investigated could be extracted, which were q = +59.5e for a single EcoRI and q = -14e for a single RecA.[48]

In 2013, Laohakunakorn et al. investigated the interactions between multiple DNA strands inside of a nanopore.[45] It was argued that in real environments, such as biological cells or

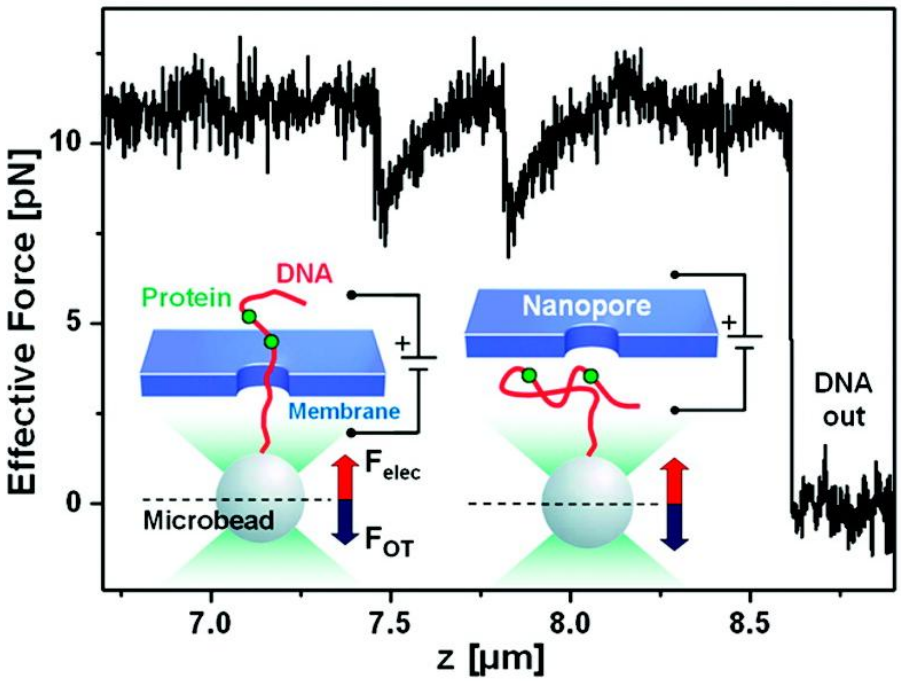

Figure 15: Schematic of the single-molecule force spectroscopy setup using a solid-state nanopore. DNA is attached to a microbead which is subsequently trapped near the nanopore. A voltage is applied to drive the DNA through the pore, and the electrophoretic force is balanced by the optical trapping force. A constant force is measured when only DNA is in the nanopore. There is a drop in the effective force signal as the two bound proteins translocate through the pore. Once the entire DNA complex exits the pore, the effective force goes to 0 pN. Reprinted with permission from Reference 48. Copyright 2011 American Chemical Society.

gel electrophoresis, DNA is confined, and that confinement may alter the way the molecules behave. The electrophoretic force acting on single DNA molecules in solid state nanopores has been well studied, so instead, this group looked at multiple DNA molecules within a single glass nanopore under an applied potential. PS microbeads were coated with dsDNA and trapped adjacent to glass nanopipettes. Multiple current and force steps were measured, with each one corresponding to the insertion of a single dsDNA molecule. As before, the capture force was found to increase with voltage, but the interesting result was that the capture force actually increased sublinearly with voltage as the number of molecules in the pore grew. It was argued that the nonlinear dependence of capture force on the number of molecules in the pore was a result of hydrodynamic interactions between molecules. Each DNA molecule in the nanopore

acts as an electroosmotic pump, and additional DNA molecules within the nanopore increase the total electroosmotic flow. The electroosmotic flow is in the same direction as the trapping force, thus, contributing to a decrease in the measured force as more DNA molecules enter the pore.[45]

Taking a different approach to the optical tweezers combined with nanopore sensing experiment, Galla et al. investigated the effects of coating a solid state nanopore with a lipid bilayer.[46] The experimental setup involved nanopores between 6 and 70 nm drilled into silicon nitride membranes using helium-ion microscopy. Nanopores were tested with and without lipid bilayers, the lipid bilayers being employed by bursting small unilamellar vesicles on the silicon nitride membrane. To go along with experimental observations, a theoretical model was developed that took into account the electrophoretic force acting on the DNA, electroosmotic fluid flow, self-energy, concentration polarization, counterion pressure, and other nonlinear and charge-induced electrokinetic effects. Experimental and theoretical results both confirmed a decrease in threading force with increasing nanopore diameter. The reason for this is that the electrophoretic force tries to pull the DNA through the pore (opposite to the optical trapping force), but the electroosmotic flow goes in the opposite direction. Larger pores have an increased electroosmotic flow, and therefore, a decreased threading force. The electroosmotic flow mainly arises due to the fact that the silicon nitride membrane and DNA molecules are negatively charged. When the pores were coated with a lipid bilayer (essentially neutralizing the charge on the pore walls), the threading force increased significantly due to the decreased electroosmotic flow. Comparing experimental results to theory, a surface charge density for the silicon nitride nanopores of σ_m = -60 mC/m^2 and a hydrodynamic slip length for the DNA of l_{slip} = 0.5 nm were deduced.[46]

By combining this optical tweezers approach with a glass nanocapillary, Bulushev et al. were able to study the position dependent electrophoretic force acting on a DNA molecule within a nanopore.[47] Glass nanocapillaries with varying sizes, 9 to 165 nm, were investigated, and the stalling force on a DNA molecule tethered to an optically trapped bead was measured (Figure 16). The nanocapillaries were adjusted in shape and size by using electron beam irradiation. The conical shape of the nanocapillaries results in an electrophoretic driving force that depends on the DNA position inside of the nanocapillary. It was discovered that the stalling force for the DNA molecules, the force equal and opposite to the electrophoretic force, increased with decreasing nanocapillary sizes. Though this was consistent with previous solid state nanopore work, the measured stalling forces for the nanocapillaries were smaller than those measured using solid state nanopores. This smaller stall force was attributed to the shape of the nanocapillary, which can be considered to be a sequence of thin nanopores with steadily increasing diameter. As the diameter of the nanopore gets larger, the electroosmotic flow

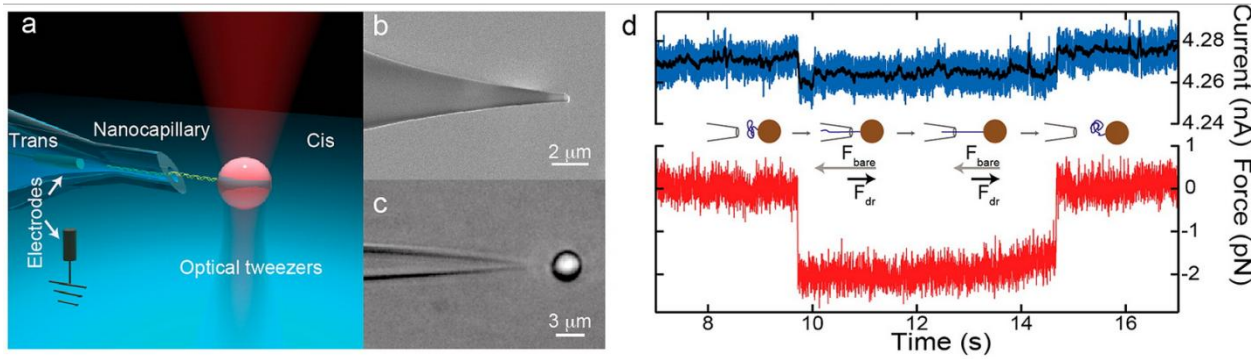

Figure 16: (A) Experimental apparatus for studying forces on DNA inside of a glass nanocapillary. DNA is attached to a microbead which is subsequently trapped near a glass nanopipette. Application of a potential difference between the two electrodes causes DNA to be forced into the pipette. (B) SEM image of a typical nanocapillary used in the experiments. (C) An optically trapped bead positioned next to the glass nanocapillary during the experiments. The position of the bead is monitored in order to calculate the effective force. (D) Experimental current and force traces showing the insertion of DNA into the nanocapillary with the initial drop of the current and force traces, the pulling of the bead away from the nanocapillary, and the reverse translocation of the DNA through the nanocapillary concomitant with the increase in current and force traces back to their original values. Reprinted with permission from Reference 47. Copyright 2014 American Chemical Society.

increases and opposes the electrophoretic force, thus decreasing the stall force. This work showed that it is possible to tune the force acting on biomolecules by adjusting the nanocapillary diameter, a rather simple approach compared to conventional solid state pores.[47]

Though extensive experimentation combining optical tweezers and solid state nanopores has been described above, there is little evidence that optical tweezers have ever been combined with αHL or any other biological nanopore for that matter. Perhaps this is because the experimental setup involved is a bit cumbersome. The closest experimental setup to a biological nanopore described above involved a lipid coated solid state nanopore.[46] The experiment described below involves combining optical tweezers with a biological nanopore embedded in a lipid bilayer membrane. It is demonstrated that it is indeed possible to optically trap a bead below a lipid bilayer suspended between two buffer reservoirs. By attaching DNA or RNA to the bead and controlling the threading of the molecule through the nanopore, it would be possible to measure the interaction forces between the naked molecules and a biological nanopore. Precise control of DNA translocation via optical tweezers could potentially have an impact on single-molecule DNA sequencing. By performing the same controlled translocation studies on protein-coated DNA and RNA molecules, one could measure the binding forces and kinetics involved.[48,49] This research could help in the understanding of disease states that arise from DNA and RNA-bound protein. For instance, the methyl binding proteins (MBPs) have been shown to play roles in cancer,[94] diabetes,[95] and immune system-related disorders.[96,97]

3.2 Methodology

3.2.1 Nanopore Setup

A custom made two chamber electrolyte holder fabricated from Teflon (Eastern Scientific LLC, Hanover, MA) is used for all nanopore experiments. A clear glass cover slip sized 24 x 60 x 1 mm (Fisher Scientific, Hampton, NH) is used for the bottom of the lower chamber so that the lipid bilayer membrane and the micropipettes can be imaged using an Observer.D1 inverted microscope (Carl Zeiss, Jena, Germany). The upper chamber is fabricated such that a Teflon partition (Eastern Scientific LLC, Hanover, MA) containing two 100 μm diameter holes, or one 100 μm diameter hole for single-molecule studies without optical tweezers, can be easily mounted on it with Kwik-Cast Silicon Elastomer (World Precision Instruments, Sarasota, FL). Before the Teflon membrane is mounted to the upper chamber, it is cleaned with pentane (Sigma Aldrich, St. Louis, MO) and dried under ambient conditions. Once attached to the upper chamber, 1 μL of a pre-paint mixture of 1 mg/mL DPhyPC (Avanti Polar Lipids, Alabaster, AL) dissolved in pentane (Sigma Aldrich, St. Louis, MO) is applied to both sides of the membrane using a dialamatic microsyringe (Drummond Scientific Co., Broomall, PA) and left to dry. The purpose of the pre-paint is to facilitate formation of the lipid bilayer membrane on the Teflon partition.

The bottom chamber is mounted on a manually manipulated microscope stage (Marzhauser Wetzlar, Wetzlar, Germany) and filled with approximately 2500 μL of either 1M KCl and 10mM TRIS solution (Sigma Aldrich, St. Louis, MO), or 1M KCl, 10mM TRIS, and 1 μM of poly-T 20mer ssDNA (Argos Technologies, Eglin, IL). The former is used for studies with the *cis*-side of the nanopore oriented upwards, while the latter is used for studies with the *trans*-side of the pore oriented upwards. The upper chamber is then placed on top of the lower

chamber and filled with approximately 650 μL of the same 1M KCl with 10mM TRIS electrolyte solution for all experiments.

For electrical measurements, Ag/AgCl electrodes are used, with one placed in each of the two chambers. The wires are prepared by dipping bare silver wire (diameter = 250 micron) into Clorox for ca. 10 minutes. Electrode wires are mounted in borosilicate or quartz micropipettes pulled with a Sutter P-2000 laser-based pipette puller (Sutter Instruments, Novato, CA). The ground electrode is mounted in the bottom chamber electrolyte solution after the micropipette is filled with the same electrolyte solution as the bottom chamber. For the single-molecule experiments, the upper electrode is either filled with 1 μM of poly-T 30mer ssDNA (Argos Technologies, Eglin, IL), 0.288 mg/mL BSA (Sigma Aldrich, St. Louis, MO), and 1M KCl with 10mM TRIS, or just a solution of 1M KCl with 10mM TRIS. The former is used for patching to the membrane when the *cis*-side of the nanopore is oriented upwards, while the latter is used for patching when the *trans*-side is oriented upwards or for a single pore in the membrane. Upper electrode tips are subsequently mounted on an Axon Instruments CV203BU headstage (Molecular Devices, Sunnyvale, CA) attached to a Sutter MP225 micromanipulator (Sutter Instruments, Novato, CA). The micromanipulators are interfaced with an MPC-200 controller (Sutter Instruments, Novato, CA). Voltages are applied and current is measured using an Axopatch 200B patch clamp amplifier (Molecular Devices, Sunnyvale, CA). A Digidata 1440A (Molecular Devices, Sunnyvale, CA) is used as an analog to digital converter and is interfaced with a National Instruments BNC-2120 plugged into a PCIe-6361 National Instruments card (National Instruments, Austin, TX). Ionic current data is collected using Clampex 10.3 software and analyzed with a custom Lab View program.

In order to form the lipid bilayer membrane, another micropipette is filled with a solution of 10 mg/mL of DPhyPC dissolved in hexadecane (Sigma Aldrich, St. Louis, MO) and subsequently mounted on another micromanipulator. The lipid micropipette is moved towards the two holes in the Teflon partition, and a FemtoJet pump (Eppendorf, Hauppauge, NY) is used to inject the lipid mixture onto the partition. A custom made glass "paintball" is then mounted on a manually operated micromanipulator (Thorlabs, Newton, NJ) and used to "paint" the lipid across the holes in the Teflon partition until a bilayer is formed on both, or just one in the case of the single-hole partition. This is typically done with a low voltage applied to facilitate bilayer formation. More lipid is injected onto the right bilayer in the two-hole partition in order to create a lipid plug.

A solution of 1 part 0.1mg/mL M1MspA (University of Washington) to 1 part 7 mg/mL BSA in water, or 1 part 0.5mg/mL αHL (Sigma Aldrich, St. Louis, MO) to 1 part 7 mg/mL BSA in water, is added to a secondary "protein pipette" tip. For experiments performed with only a single pore in the membrane, a solution of 1 μg/mL M1MspA and 1.75 mg/mL BSA is used to help prevent excess insertions. The lipid micropipette is then removed from the experimental apparatus and replaced by the "protein pipette" tip, which is either positioned directly above the bilayer membrane for *cis*-side up insertion, or inserted through the membrane for *trans*-side up insertion. A compensation pressure of 30-40 hPa is applied to gently blow the protein out of the tip until approximately 300-500 αHL pores, or 100-150 MspA pores, insert into the membrane. For the single MspA insertion, small pressure pulses of 100-150 hPa and 0.2-0.5 s duration are used, followed by several minutes of waiting, until a single insertion is observed. If multiple pores insert, the membrane is repainted and the process started again. Pore insertion is confirmed via current measurement.

The initial αHL and MspA studies require only patching onto a single pore with the upper electrode, or inserting a single pore via the pressure method. All of the initial steps are observed using a Zeiss N-Achroplan 10x objective with a numerical aperture (NA) of 0.25 (Carl Zeiss, Jena, Germany). Video is capture using a Thorlabs USB 2.0 digital camera (Thorlabs, Newton, NJ) attached to the microscope. Figure 17 shows a schematic of the experimental apparatus.

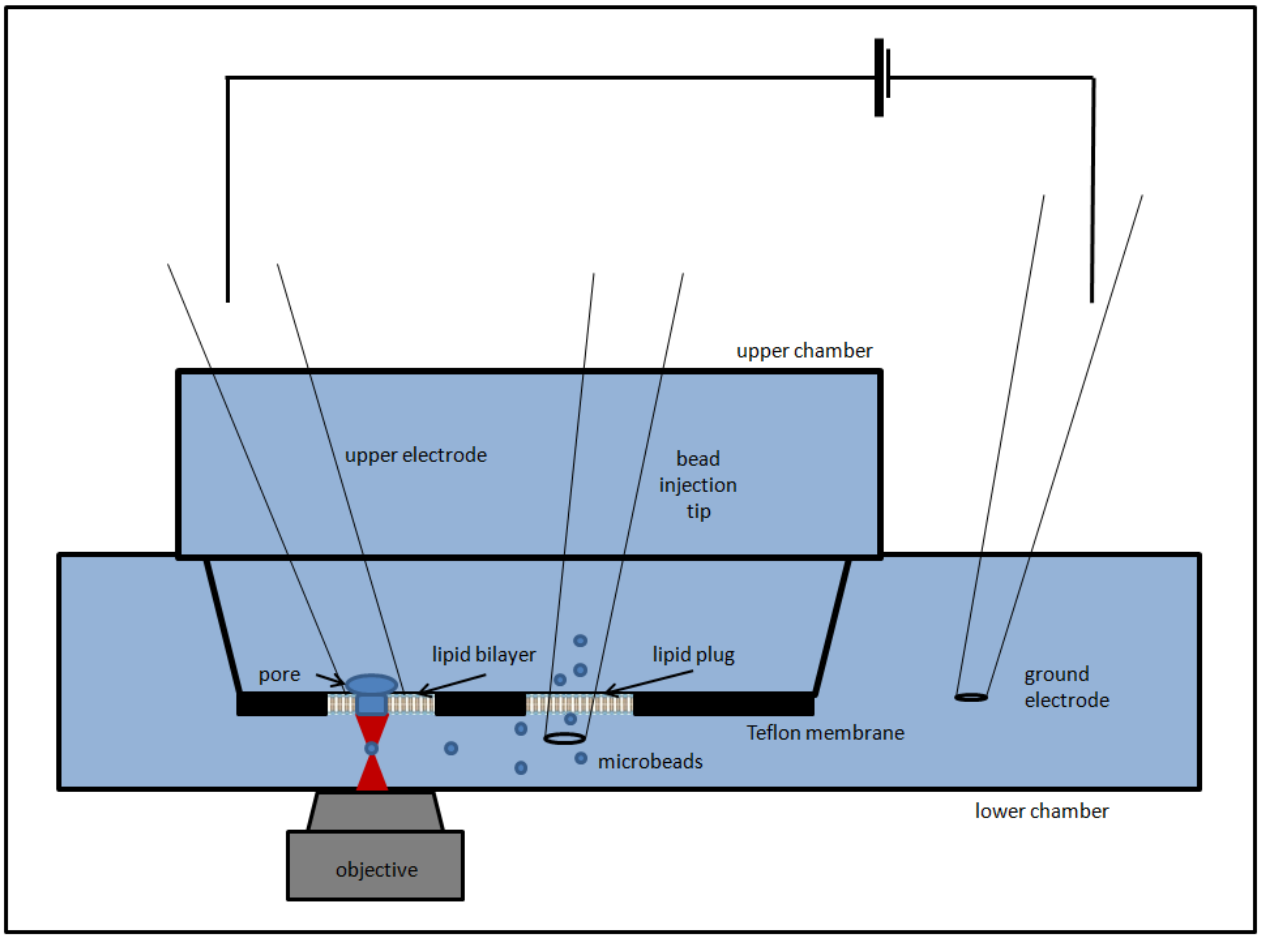

Figure 17: Schematic of the experimental apparatus with the two-hole partition used for bead injection. For experiments, microbeads are injected below the membrane using the bead injection tip, which is inserted through the lipid plug on the right. The upper electrode is patched onto a single nanopore once a bead is trapped. The patch tip is then manipulated towards the bead and a transmembrane voltage applied. For initial single-molecule MspA experiments, the partition with a single hole is used and either the patch tip or the lower chamber is filled with ssDNA, for the *cis*-side up and *trans*-side up experiments respectively. For experiments with a single pore in the membrane, the upper electrode tip is not patched to the membrane.

3.2.2 Optical Tweezers

A continuous wave diode pumped solid state (CW DPSS) laser (CrystaLaser, Reno, NV) that outputs 700mW at 1064nm is used as the trapping laser. Thorlabs PF10-03-P01 mirrors (Thorlabs, Newton, NJ) are mounted on New Focus 9807 mirror mounts (New Focus, Santa Clara, CA) and used to direct the incident laser light through 50 cm, 10 cm, 25 cm focal length PCX BK7, IR coated lenses (Newport, Irvine, CA), which were chosen to collimate and expand the beam to overfill the back aperture of the objective. The beam is then reflected off of an XB12 laser rejection filter (Horiba, Kyoto, Japan) before being sent into the microscope, allowing it to be sent into the optical train collinear with the detection laser. An XF2014 610DRLP dichroic mirror (Omega Optical, Brattleboro, VT) is used to send the laser light through a Zeiss 100x Plan-Apochromat oil immersion objective with an NA of 1.4 (Carl Zeiss, Jena, Germany). The focused laser light is used to trap the PS microbeads (Spherotech, Lake Forest, IL) in the bottom chamber, and the beads are manipulated in solution using the microscope stage.

A second CW DPSS laser (CrystaLaser, Reno, NV) that outputs 20mW at 640nm is used for particle tracking measurements. An LD01-640/8-12.5 MaxDiode filter (Semrock, Rochester, NY) is used to clean up the laser beam. New Focus 5101 VIS mirrors (New Focus, Santa Clara, CA) are mounted on New Focus 9807 mirror mounts and used to direct the incident laser light through the XB12 laser rejection filter into the back of the microscope. An XF2014 610DRLP dichroic mirror is used to send the laser light through the Zeiss 100x Plan-Apochromat oil immersion objective. Backscattered light from trapped beads is collected with the objective, sent out of the microscope, and then through an f = +10 cm lens. The lens is mounted on an adjustable mount from Thorlabs so the image of the bead could be adjusted for maximum signal from the 2911 Quadrant Photodiode (QPD) (New Focus, Santa Clara, CA). The QPD itself is

mounted onto a rotating mount (Thorlabs, Newton, NJ) in order to align the translation coordinates of the trapped beads with the axes of the QPD. An FF02-6755/67-25 BrightLine single-band bandpass filter (Semrock, Rochester, NY) is placed in front of the QPD to block unwanted light. The QPD is connected to the National Instruments BNC-2120 and interfaced with the computer via the PCIe-6361 National Instruments card. Voltage signals are monitored and recorded with a custom LabVIEW program. A schematic of the optical train can be seen in Figure 18.

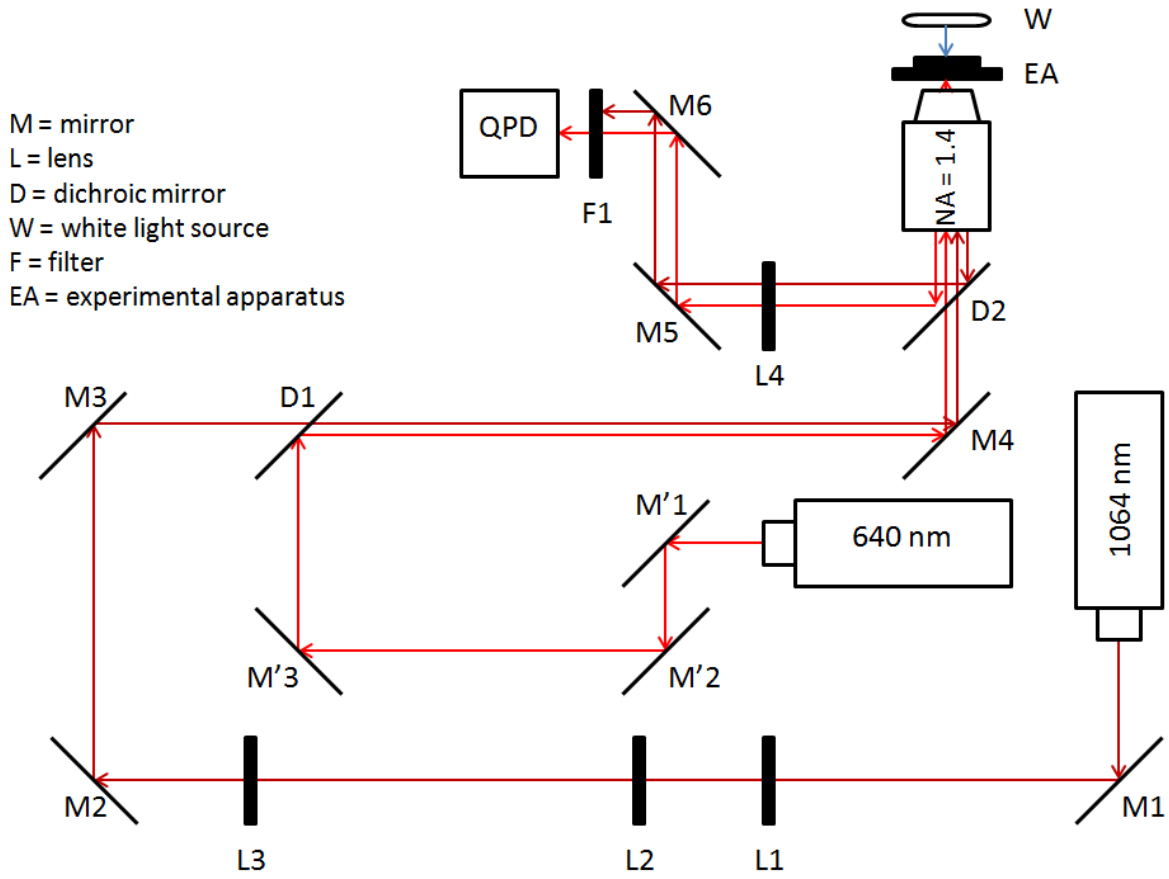

Figure 18: Schematic of the force measurement optical train, not drawn to scale. The lenses listed above have focal lengths: L1, *f* 1 = 50 cm; L2, *f* 2 = 10 cm; L3, *f* 3 = 25 cm; L4, *f* 4 = 10 cm. The primes denote parts that are solely used for the force measurement laser. After D1, both beams are collinear but are shown with an offset for clarity. Detailed descriptions of the parts are described in the above section.

3.3 Results and Discussion

3.3.1 Trapping Beads Underneath of a Biological Membrane

The experimental setup has to be slightly modified from typical biological nanopore experiments in order to accommodate the streptavidin coated beads below the lipid bilayer membrane. Beads were originally placed into the lower electrolyte chamber initially to be trapped after the membrane was painted and a pore was patched onto. However, in the time that it took to do that, the concentration of beads directly below the membrane diminished substantially, making it extremely hard to find beads to trap. In order to overcome this obstacle it was necessary to switch to the two-hole Teflon membrane partition seen in Figure 19. This

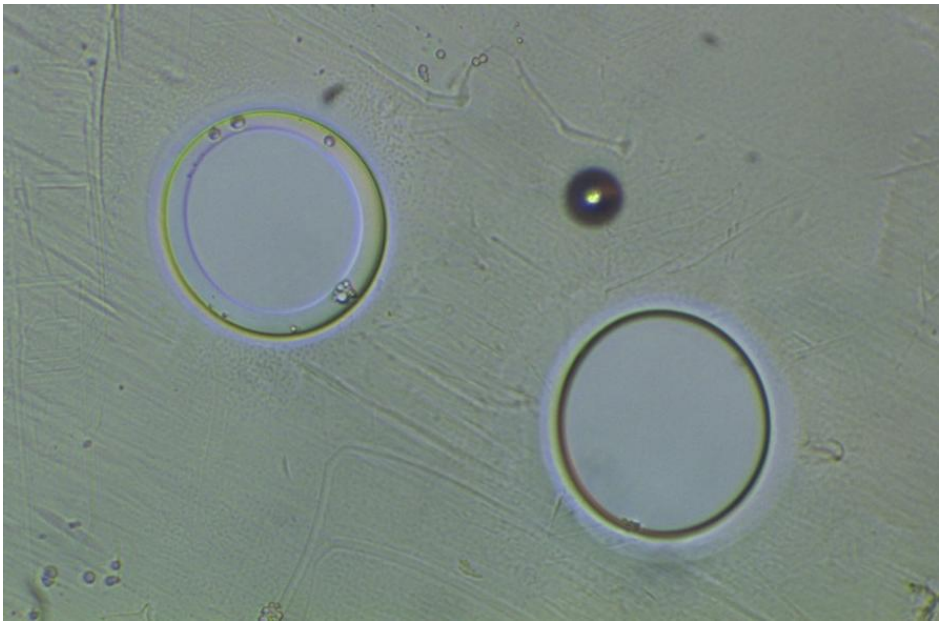

Figure 19: Teflon membrane partition used for trapping experiments with two 100 μm holes. The left hole in the figure has a lipid bilayer membrane painted across it, as evidenced by the annulus near the edge of the hole. The right hole is plugged with lipid. This allows for insertion of αHL into the left membrane, while the right membrane is used for insertion of the bead injection tip below the membrane.

allows for the formation of a lipid bilayer over one of the holes and a lipid plug over the other. The nanopores are injected into the bilayer membrane, while the lipid plug is used so that a bead injection tip can be manipulated below the membrane.

A custom program was designed in order to pull micropipette tips with a large enough diameter to inject the beads without getting clogged. Once the lipid membrane is formed, the bead tip is inserted through the lipid plug and beads are injected below the membrane (Figure 20). The addition of the bead injection tip allows for on demand injection of beads so that multiple experiments can be performed before breaking down the apparatus. After injection of beads, the bead tip is manipulated back through the lipid plug and out of the way.

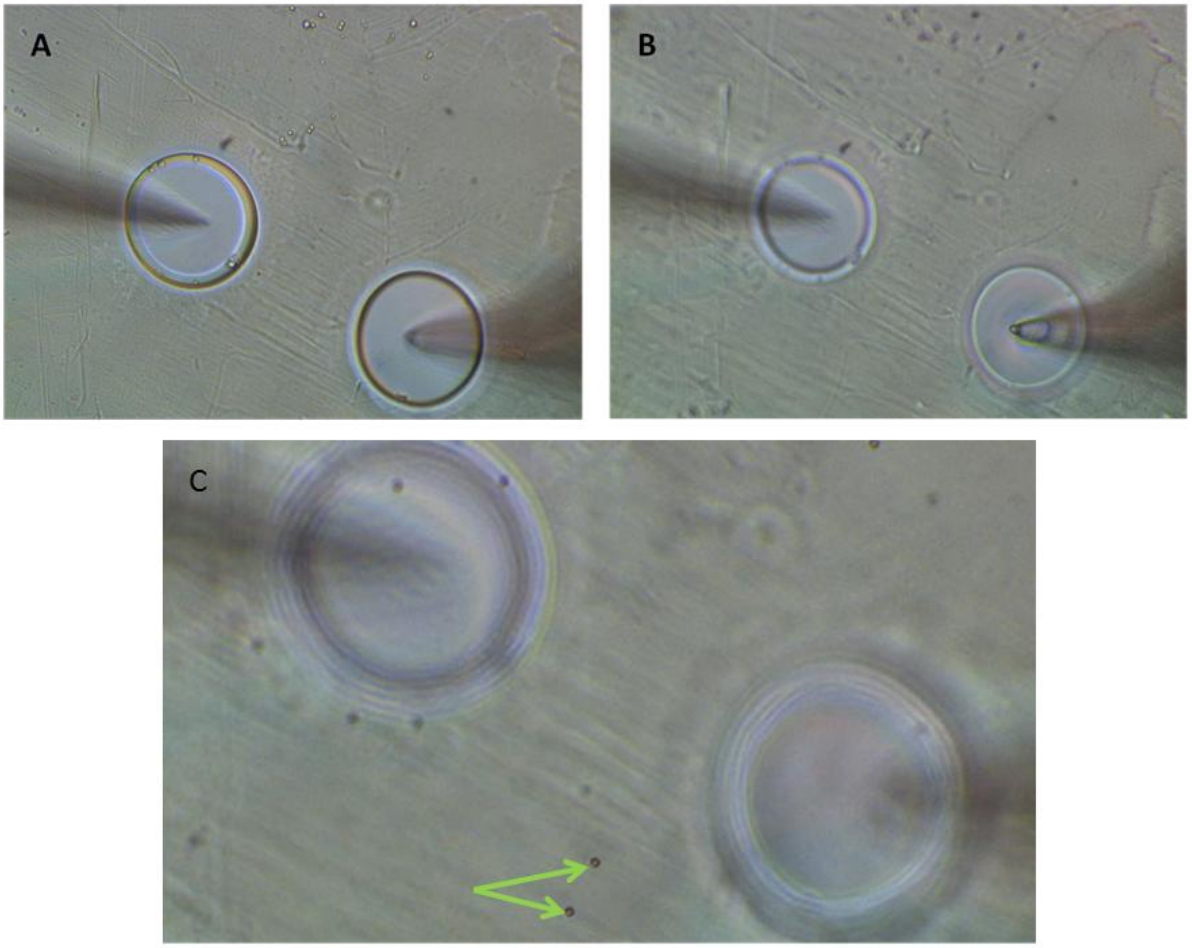

Figure 20: Procedure for delivering beads underneath of a biological membrane. (A) An electrode tip is placed above the lipid bilayer membrane on the left hand side, while the bead injection tip is positioned over the lipid plug on the right hand side. (B) The bead injection tip is manipulated through the lipid plug and refocused below the membrane. (C) Streptavidin coated beads 5 μm in diameter are injected below the membrane by applying a continuous backing pressure to the bead injection tip. The bead tip is then pulled back through the lipid plug to stop convective flow below the membrane. The green arrows indicate the position of two PS beads. The holes in the partition are 100 μm in diameter for comparison.

3.3.2 Demonstration of Simultaneous Trapping and Nanopore Current Blockade Measurements

In order to trap a bead it is necessary to switch over to the 1.4 NA 100x objective, which allows for the infrared laser beam to be more tightly focused. At this point, the trapping laser is turned on and the microscope stage manipulated until a single bead falls into the trap. The bead is then brought within a few microns of the lipid bilayer membrane by focusing upwards (Figure 21). With the bead in place, the upper chamber electrode tip is patched onto a single nanopore, which is confirmed by current measurements.

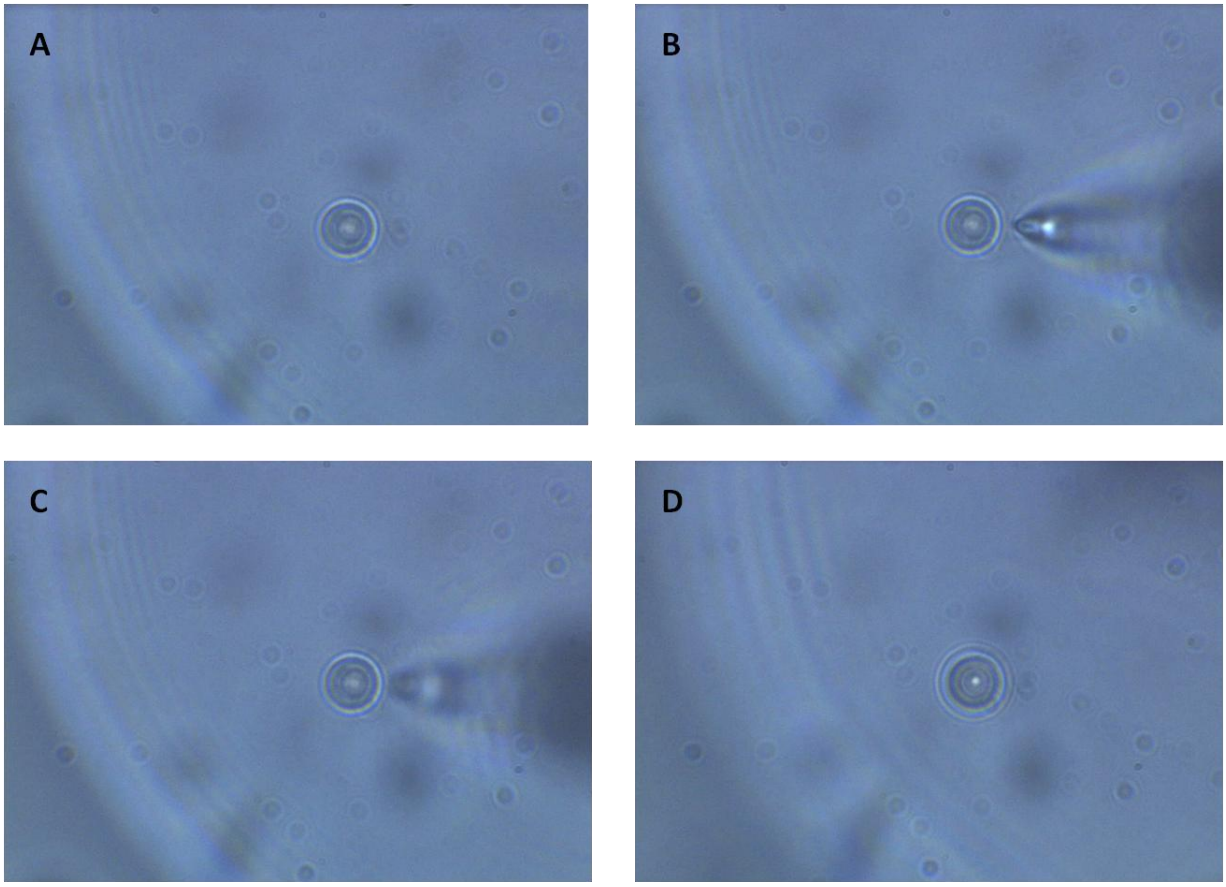

Figure 21: Manipulation of the PS bead trapped below the membrane. (A) The trapped bead is brought closer to the membrane by focusing upwards. (B) The nanopore patch tip is brought downwards and into focus next to the bead. (C) The patch tip is then raised slightly to facilitate the translocation of ssDNA into the nanopore at the proper angle. (D) After the experiment, the patch tip is pulled upwards and away from the bead, and the bead can be manipulated towards a new pore for another experiment.

As proof of principle, some initial current blockade studies were performed with a bead trapped below the pore. The bilayer membrane was injected with αHL nanopores as described in the methods section. When approximately 300-500 pores were confirmed by current measurements, beads were injected below the partition, and a single bead was trapped. The electrode tip, filled with ssDNA analyte, was patched onto a single pore and then manipulated down towards the trapped bead. A negative voltage was applied to force the negatively charged ssDNA through the *cis*-side of the pore. Representative current traces are shown in Figure 22.

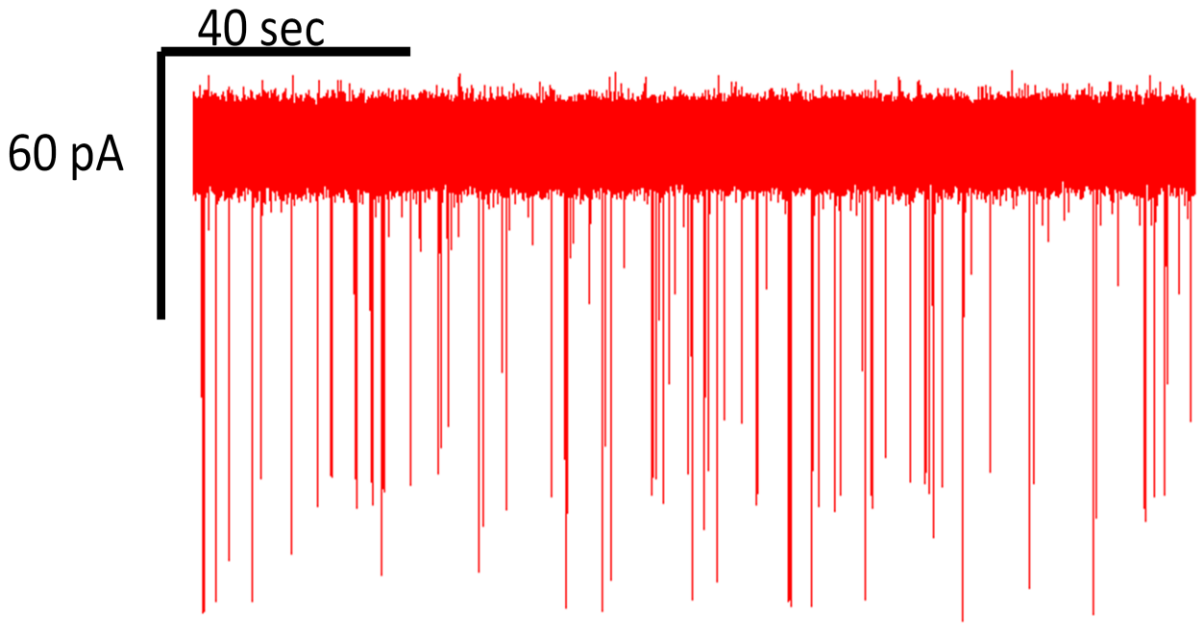

Figure 22: Representative current trace during the experiment showing the interaction of ssDNA with the nanopore and subsequent blockades at -100 mV applied potential in 1M KCl.

3.3.3 Optical Tweezers Force Calibration

The goal is to thread a DNA molecule bound to a trapped bead through a pore to measure the force on the DNA while in the pore. This requires an accurate calibration of the force on the bead as a function of the displacement of the bead. To find the force acting on an optically

trapped bead it is necessary to determine the spring constant k of the optical trap. The spring constant can be determined by observing the Brownian motion of the trapped bead. According to the Einstein-Ornstein-Uhlenbeck theory, the Brownian motion can be described by the Langevin equation:

$$m\frac{d^2x(t)}{dt^2} + \gamma\frac{dx(t)}{dt} + kx(t) = \eta(t) \tag{13}$$

where the position and the mass of the particle are given by $x(t)$ and m respectively, $-kx(t)$ is the harmonic force of the trap, $\eta(t)$ encompasses the random thermal force on the particle felt during Brownian motion at temperature T, and γ is given by the Stoke's drag coefficient for spherical particles:

$$\gamma = 6\pi\mu r \tag{14}$$

where μ is the dynamic viscosity of the medium, and r is the radius of the particle.[98]

Typically, the inertial term of Equation 13 can be neglected since loss of kinetic energy through friction is orders of magnitude shorter than the experimental time resolution. [98] Thus, Equation 13 becomes:

$$\gamma\frac{dx(t)}{dt} + kx(t) = \eta(t). \tag{15}$$

If $\eta(t)$ is truly a random process due to thermal fluctuations, then its average value is zero and its power spectrum is a constant given by:

$$|\eta(f)|^2 = 4\gamma k_B T \tag{16}$$

where k_B is Boltmann's constant and T is the temperature. The solution to Equation 15 can be found by taking the Fourier transform of both sides:

$$2\pi\gamma(f_c - if)X(f) = \eta(f)\,. \tag{17}$$

The modulus of Equation 17 yields a relationship between the power spectrum of the trapped particle and the corner frequency:

$$|X(f)|^2 = \frac{k_B T}{\pi^2\gamma({f_c}^2 + f^2)}\,. \tag{18}$$

where the corner frequency of the optical trap has been defined by:

$$f_c \equiv \frac{k}{(2\pi\gamma)}\,. \tag{19}$$

By determining the corner frequency of the optical trap using the power spectrum, it is then possible to determine the spring constant of the harmonic potential well and to relate the change in position of the bead to the forces acting upon it.[99]

Calibration of the optical trap is performed by trapping 3 μm PS microbeads and monitoring their position for an extended period of time. This signal is then average and converted into to a power spectrum. The corner frequency described in Equation 19 is obtained from a Lorentzian least squares fit of the power spectrum in Figure 23, $f_c = 57.7 \pm 0.1$ Hz.[99] From the corner frequency it is possible to calculate the spring constant of the trapping laser, $k =$ (9.1 ± 0.1) x 10^{-3} pN/nm, using Equations 14 and 19. Knowing the voltage changes for different bead displacements and the spring constant of the trap, it is possible to determine the forces exerted on the optically trapped bead during the proposed experiments.

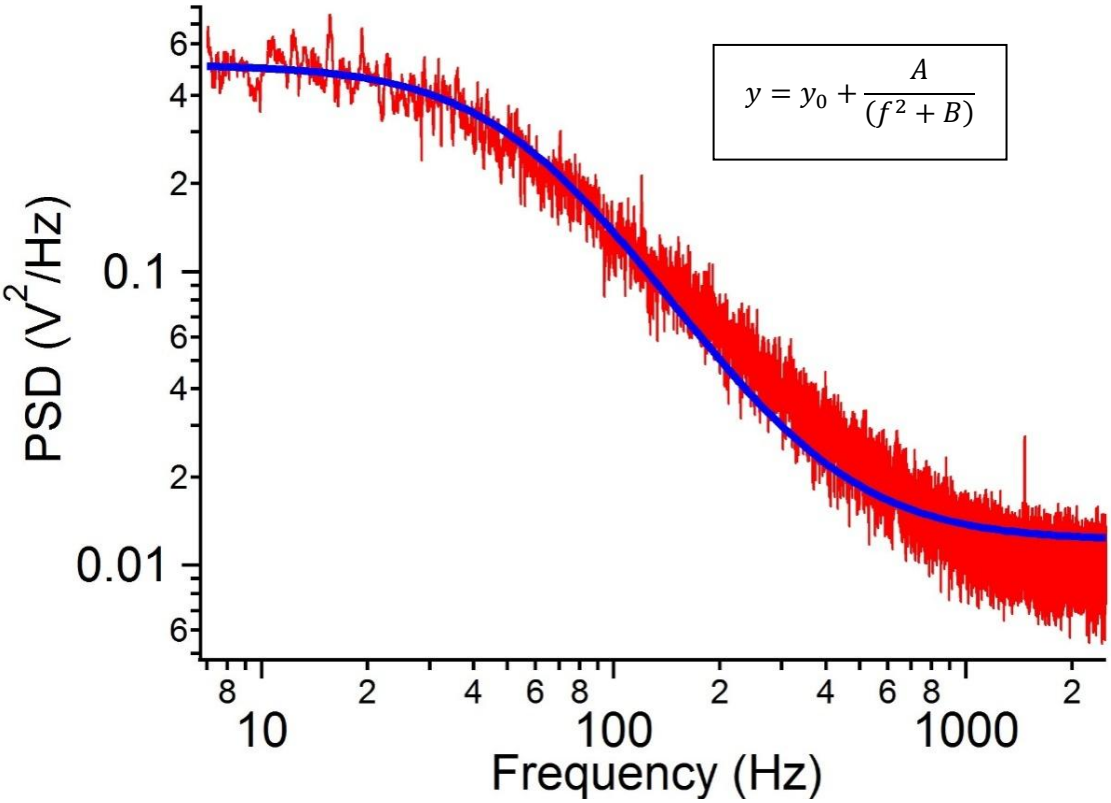

Figure 23: Lorentzian power spectrum of a 3 μm PS bead moving within an optical trap at a power of 700mW. The QPD x-axis voltage values were recorded for approximately 100 seconds, from which ten power spectrums of ten second periods each were taken and averaged to produce the above spectrum. The power spectrum is fit with the Lorentzian function shown in the box, with the fitting parameters: $y_0 = 60.7 \pm 0.1$, $A = (8.27 \pm 0.01)$ x 10^{-6}, and $B = 3323.6 \pm 3.59$. The corner frequency is obtained from the square root of B, $f_c = 57.7 \pm 0.1$ Hz,[99] which can be combined with Equations 14 and 19 to find the spring constant of the trap $k = (9.1 \pm 0.1)$ x 10^{-3} pN/nm.

With the current experimental apparatus, it has been demonstrated above that it is possible to optically trap PS microbeads within a few microns of a biological nanopore embedded in a lipid bilayer membrane. Thus, it may be possible to measure the pulling force on ssDNA through a properly sized biological nanopore, MspA or αHL for example. As a first attempt at mimicking the geometry of the experimental arrangement and acquiring force data, a pipette tip was positioned close to a trapped bead and small pressure pulses were applied (Figure 24).

The pipette tip is at an angle, so the pressure pulses tend to displace the bead to the left and downwards. A position laser is overlapped with the trapping laser and backscattered light off of the trapped bead is fed into the QPD to monitor motion of the bead. By observing the voltage

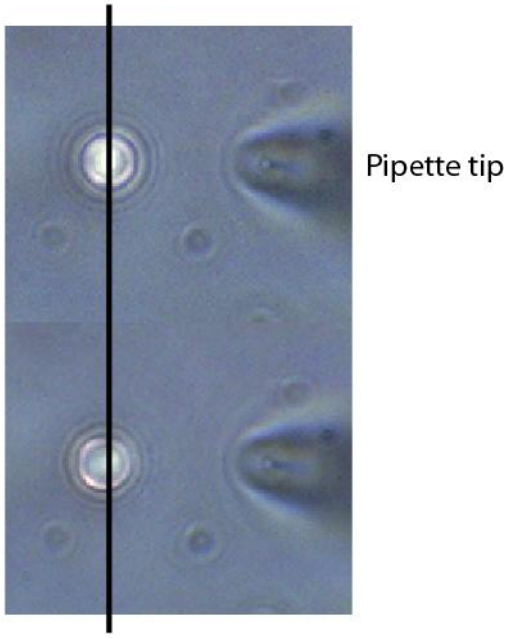

Figure 24: Video images of a 3 μm trapped bead under the influence of a force from the pipette tip. The top image shows the undisturbed bead and the bottom picture shows the bead undergoing a slight displacement as a result of the applied pressure at the tip (25 hPa). The geometry of this arrangement mimics the experimental conditions used in the nanopore measurement.

traces obtained from the QPD, the displacements of the bead can be correlated with the particular pressure pulses applied. Figure 25 shows a sequence of pressure pulses starting at 15 hPa and increasing in 5 hPa increments until the bead is ejected from the trap at an injection pressure of 30 hPa.

From this data it is possible to calculate the lower threshold force limit of detection of the apparatus. This done by approximating the velocity v at the end of the pipette tip with a simplified Bernoulli equation for an incompressible fluid with no height difference:

$$v = \sqrt{\frac{2P}{\rho}} \tag{20}$$

where P is the applied pressure and ρ is the density of the fluid. Combining this with the Stokes' drag force F for a sphere moving in a fluid at velocity v:

$$F = 6\pi\mu r v \tag{21}$$

where μ is the dynamic viscosity of the fluid, and r is the radius of the sphere, allows for an approximation of the force on the bead. By measuring the voltage changes recorded with the

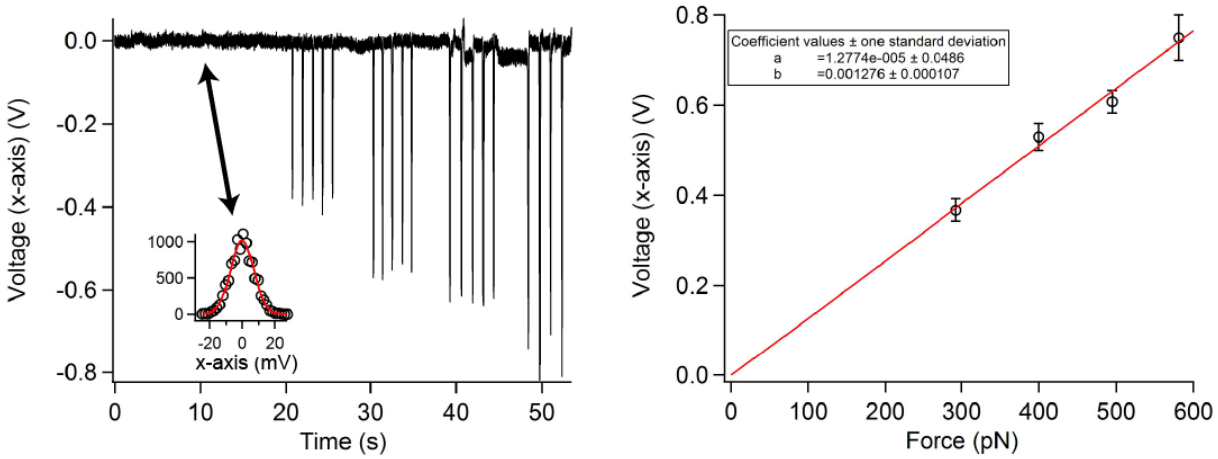

Figure 25: (Left) At t = 0 s, a 3 μm bead is trapped near the end of a micropipette tip and position fluctuations along the x-axis are monitored. Starting at $t \approx 20$ s pressure pulses are applied to the tip. The pulses push the bead in the x- and z- directions, which give rise to sharp downward spikes in the photodiode's x-axis voltage output. Five pulses are applied at each pressure (15 hPa – 30 hPa in 5 hPa steps). The inset graph shows the all-points histogram of the current before the pulses are applied. The width of this histogram (20 mV) sets the lower limit of voltage detection at the sampling frequency used (500 Hz). (Right) The tip pulse pressures are converted to force with the Stokes and Bernoulli relationships ($F = 6\pi\mu Rv$ and $v = \sqrt{(2P/\rho)}$). A linear relationship between the bead's x-axis displacement and the applied force is found, with the slope of this line equal to1.28 mV/pN. Combining this with the 20 mV width seen in the left inset, sets the force threshold detection limit at 20/1.28 = 15.6 pN.

QPD at different applied pressures and converting those pressures to forces, a linear relationship between force and voltage is obtained (Figure 25). Combining the slope of this line, 1.28 mV/pN, with the width of the all points histogram, 20 mV, at a sampling frequency of 500 Hz, allows for the calculation of the lower threshold force limit of detection, (20 mV)/(1.28 mV/pN) = 15.6 pN. This is well below the expected force required for a ssDNA molecule in an MspA pore, 50-60pN, showing that the apparatus is indeed capable of performing the proposed force measurement experiments.

3.3.4 Initial MspA Single-Molecule Studies

Before an experiment is performed to directly measure the forces between an MspA nanopore and an ssDNA molecule, it would helpful to understand the basic interactions between single-molecules and MspA. This initial information is gathered by performing routine single-molecule current blockade studies with the MspA nanopore suspended in a lipid bilayer membrane. The pore is first inserted into the membrane with the *cis*-side oriented towards the upper chamber. In this direction, it is necessary to patch onto the membrane with an electrode that contains the ssDNA to be studied. Once a single pore is confirmed, a series of voltages, ranging from -140 mV to 140 mV, are applied and current traces are recorded. To better understand the characteristics of translocation, the pore is then inserted into the membrane with the *trans*-side oriented upwards, while the ssDNA is loaded into the bottom chamber of the experimental apparatus. The same voltage studies are repeated, and representative current blockade data can be seen in Figure 26.

Further study with a single MspA inserted into the membrane is also performed. To do this, it is necessary to dilute the MspA in the protein insertion tip by a factor of 100. The protein

insertion tip is then brought close to the membrane and small pressure pulses applied until a single insertion is observed. Once a single insertion is confirmed, an I-V curve is taken before

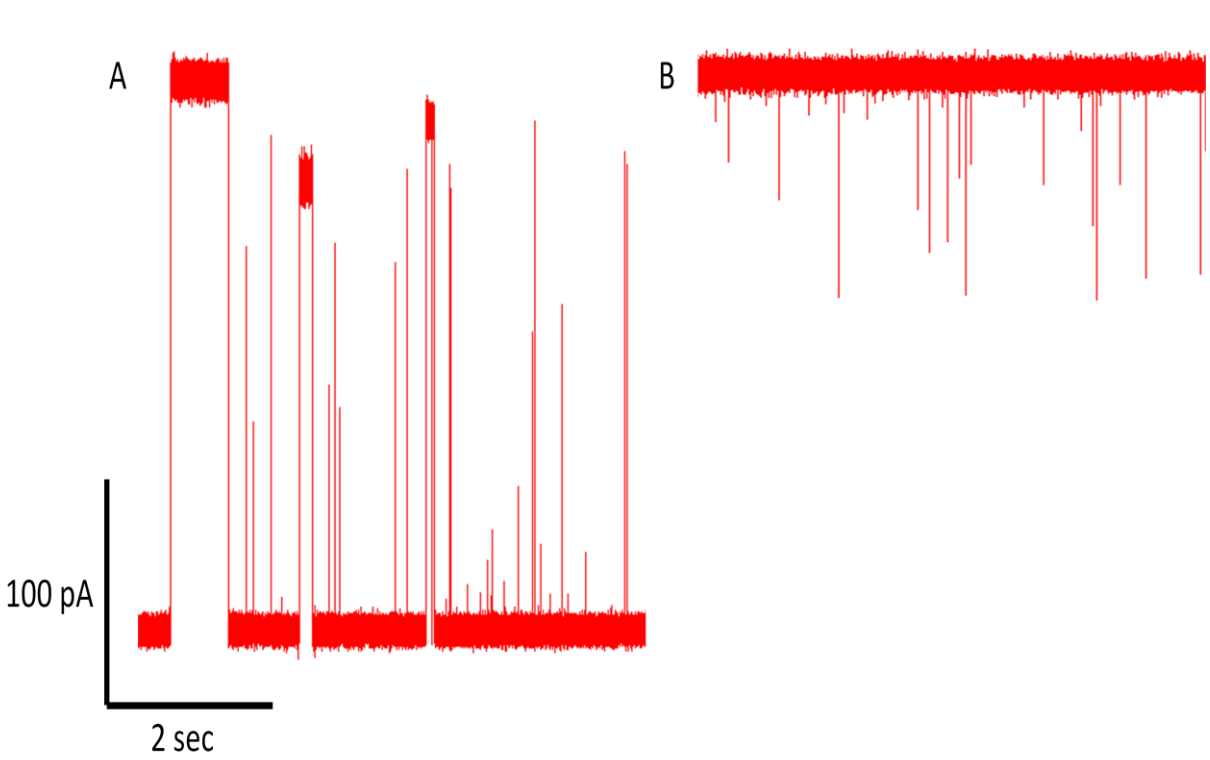

Figure 26: Representative ssDNA current blockade data taken with MspA in 1M KCl. (A) Data taken with the *cis*-side oriented upwards and 1 μM of poly-T 30mer in the patch electrode tip with -100mV applied voltage. (B) Data taken with the *trans*-side oriented upwards and 1 μM of poly-T 20mer in the bottom chamber with 100mV applied potential.

analyte is injected into the solution (Figure 27). The slope of the linear regression fit to the I-V curve and its inverse give a resistance of 407 ± 5 MΩ and a conductance of 2.46 ± 0.03 nS, respectively, at 1M KCl and ~21^{o}C. This is consistent with the reduction of conductance by a factor of 2-3 for M1MspA as compared to the value of 4.9 nS in 1 M KCl at ~20^{o}C previously reported for wild-type MspA.[68] Another micropipette is then filled with a mixture of 5 μM poly-T 20mer ssDNA and is used to controllably inject the ssDNA near the pore mouth. A series of voltages from -140 mV to 140 mV is run while ssDNA is being injected, and current blockade

data is recorded. This data will be used as a baseline for future force measurement experiments with MspA.

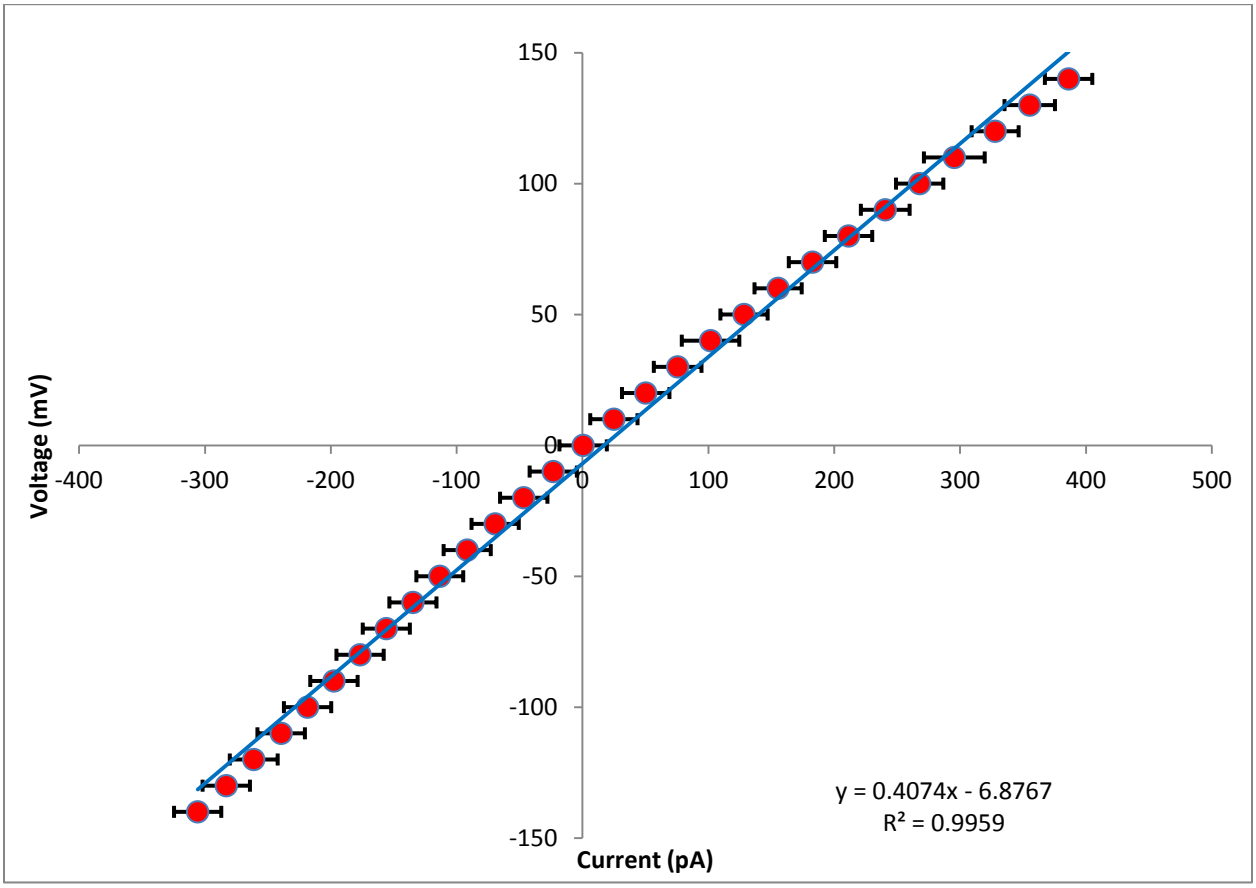

Figure 27: I-V curve of a single M1MspA channel. An asymmetry can be seen when the voltage polarity is flipped. The slope of the linear regression fit and its inverse give a pore resistance of 407 ± 5 MΩ and a conductance of 2.46 ± 0.03 nS, respectively, at 1M KCl and ~21^{o}C.

3.4 Conclusions

It has been demonstrated that optical tweezers can be coupled with a biological nanopore system. The initial obstacles to this particular apparatus have been overcome, and a well-developed method has been established for conducting future experiments with tweezers and biological nanopores. For example, many of the experiments discussed in the introduction to this chapter could be reinvestigated with a biological nanopore. A simple next step would involve attaching biotinylated ssDNA molecules to streptavidin coated beads and trapping one below the

lipid membrane. This is currently being undertaken by our collaborators at the University of Washington (PI Jens Gundlach). The bead could be manipulated towards the membrane while a voltage is applied to drive the ssDNA through the nanopore. The forces acting on the ssDNA could be measured by monitoring the bead's position in the trap, thus allowing characterization of the forces imparted on analyte molecules while translocating through biological nanopores. This would be the first direct force measurement using optical tweezers and a biological nanopore of its kind.

References

[1] J. J. Kasianowicz, E. Brandin, D. Branton, and D. W. Deamer, *P. Natl. Acad. Sci. USA* **93**, 13770 (1996).

[2] J. Griffiths, *J. Anal. Chem.* **80**, 23-27 (2008).

[3] S. Howorka and Z. Siwy, *Chem. Soc. Rev.* **38**, 2360 (2009).

[4] L. Movileanu, *Trends Biotechnol.* **27**, 333 (2009).

[5] H. Wang, Y. Ying, H. Kraatz, and Y. Long, *Anal. Chem.* **83**, 1746 (2011).

[6] A. Boersma and H. Bayley, *Angew. Chem. Int. Ed.* **51**, 9606 (2012).

[7] L. Gu, O. Braha, S. Conlan, S. Cheley, and H. Bayley, *Nature* **398**, 686 (1999).

[8] Y. Wang, D. Zheng, Q. Tan, M. Wang, and L. Gu, *Nat. Nanotechnol.* **6**, 668 (2011).

[9] D. Wang, Q. Zhao, R. S. S. de Zoysa, and X. Guan, *Sensor. Actuat. B-Chem.* **139**, 440 (2009).

[10] X. Guan, L. Gu, S. Cheley, O. Braha, and H. Bayley, *ChemBioChem* **6**, 1875 (2005).

[11] O. Braha, L. Gu, L. Zhou, X. Lu, S. Cheley, and H. Bayley, *Nat. Biotechnol.* **18**, 1005 (2000).

[12] H. Wu and H. Bayley, *J. Am. Chem. Soc.* **130**, 6813 (2008).

[13] M. V. Hout, I. D. Vilfan, S. Hage, and N. H. Dekker, *Nano Lett.* **10**, 701 (2010).

[14] M. Boccalon, E. Iengo, and P. Tecilla, *J. Am. Chem. Soc.* **134**, 20310 (2012).

[15] J. Clarke, H. Wu, L. Jayasinghe, A. Patel, S. Reid, and H. Bayley, *Nat. Nanotechnol.* **4**, 265 (2009).

[16] W. H. Coulter, US Pat., 2656508 (1953).

[17] S. B. Hladky and D. A. Haydon, *Nature* **225**, 451 (1970).

[18] E. Neher and B. Sakmann, *Nature* **260**, 799 (1976).

[19] H. Bayley and C. R. Martin, *Chem. Rev.* **100**, 2575 (2000).

[20] N. G. Stanley-Wood and R. W. Lines, *Particle Size Analysis*, Royal Society of Chemistry, London, 1992.

[21] P. Mueller, D. O. Rudin, H. T. Tien, and W. C. Wescott, *Nature* **194**, 979 (1962).

[22] O. P. Hamill, A. Marty, E. Neher, B. Sakmann, and F. J. Sigworth, *Pfluegers Arch.* **391**, 85 (1981).

[23] B. Hille, *Ion Channels of Excitable Membranes*, Sinauer Associates, 2001.

[24] B. Sakmann and B. Neher, *Single Channel Recording*, Plenum Press, New York, 1995.

[25] C. Miller, *Ion Channel Reconstitution*, Springer, New York, 1986.

[26] R. I. Hume, L. W. Role, and G. D. Ficshbach, *Nature* **305**, 632 (1983).

[27] T. G. Allen, *Trends Neurosci.* **20**, 192 (1997).

[28] H. Bayley, T. Luchian, S. H. Shin, and M. Steffensen, *Single Molecules and Nanotechnology*, Springer, Berlin Heidelberg, Germany, 2008.

[29] S. McGinn and I. G. Gut, *Nat. Biotechnol.* **30**, 366 (2013).

[30] L. Ma and S. L. Cockroft, *ChemBioChem* **11**, 25 (2010).

[31] H. Y. Wang, Y. L. Ying, Y. Li, and Y. T. Long, *Chem. Asian. J.* **5**, 1952 (2010).

[32] J. E. Reiner, A. Balijepali, J. W. F. Robertson, B. S. Drown, D. L. Burden, and J. J. Kasianowicz, *J. Chem. Phys.* **137**, 214903 (2012).

[33] S. Majd, E. C. Yusko, Y. N. Billeh, M. X. Macrae, J. Yang, and M. Mayer, *Cur. Opin. Biotechnol.* **21**, 439 (2010).

[34] A. S. Perera, H. Wang, M. T. Basel, M. R. Pokhrel, P. S. Gamage, M. Kalita, S. Wendel, B. Sears, D. Welindeniya, Y. Liu, C. Turro, D. Troyer, and S. H. Bossman, *Langmuir* **29**, 308 (2012).

[35] I. M. Derrington, T. Z. Butler, M. D. Collins, E. Manrao, M. Pavlenok, M. Niederweis, and J. H. Gundlach, *P. Natl. Acad. Sci. USA* **107**, 16060 (2010).

[36] A. H. Laszlo, I. M. Derrington, H. Brinkerhoff, K. W. Langford, I. C. Nova, J. M. Samson, J. J. Bartlett, M. Pavlenok, and J. H. Gundlach, *P. Natl. Acad. Sci. USA* **110**, 18904 (2013).

[37] E. A. Manrao, I. M. Derrington, A. H. Laszlo, K. W. Langford, M. K. Hopper, N. Gillgren, M. Pavlenok, M. Niederweis, and J. H. Gundlach, *Nat. Biotechnol.* **30**, 349 (2012).

[38] E. A. Manrao, I. M. Derrington, M. Pavlenok, M. Niederweis, and J. H. Gundlach, *PLOS One* **6**, 1 (2011).

[39] T. J. Jeon, N. Malmstadt, and J. J. Schmidt, *J. Am. Chem. Soc.* **128**, 42 (2006).

[40] J. W. Shim and L. Q. Gu, *Anal. Chem.* **79**, 2207 (2007).

[41] X. F. Kang, S. Cheley, A. C. Rice-Ficht, and H. Bayley, *J. Am. Chem. Soc.* **129**, 4701 (2007).

[42] J. E. Reiner, J. J. Kasianowicz, B. J. Nablo, and J. W. F. Robertson, *P. Natl. Acad. Sci. USA* **107**, 12080-12085 (2010).

[43] U. F. Keyser, B. N. Koeleman, S. V. Dorp, D. Krapf, R. M. M. Smeets, S. G. Lemay, N. H. Dekker, and C. Dekker, *Nat. Phys.* **2**, 473 (2006).

[44] U. F. Keyser, J. van der Does, C. Dekker, and N. H. Dekker, *Rev. Sci. Instrum.* **77**, 105105 (2006).

[45] N. Laohakunakorn, S. Ghosal, O. Otto, K. Misiunas, and U. F. Keyser, *Nano Lett.* **13**, 2798 (2013).

[46] L. Galla, A. J. Meyer, A. Spiering, A. Sischka, M. Mayer, A. Hall, P. Reimann, and D. Anselmetti, *Nano Lett.* **14**, 4176 (2014).

[47] R. D. Bulushev, L. J. Steinbock, S. Khlybov, J. F. Steinbock, U. F. Keyser, and A. Radenovic, *Nano Lett.* **14**, 6606 (2014).

[48] A. Spiering, S. Getfert, A. Sischka, P. Riemann, and D. Anselmetti, *Nano Lett.* **11**, 2978 (2011).

[49] A. Sischka, A. Spiering, M. Khaksar, M. Laxa, J. Konig, K. J. Dietz, and D. Anselmetti, *J. Phys. Condens. Matter* **22**, 454121 (2010).

[50] A. M. Maxam and W. Gilbert, *Proc. Natl. Acad. Sci. USA* **74**, 560 (1977).

[51] F. Sanger, S. Nicklen, and A. R. Coulson, *Proc. Natl. Acad. Sci. USA* **74**, 5463 (1977).

[52] D. A. Wheeler, M. Srinivasan, M. Egholm, Y. Shen, L. Chen, A. McGuire, W. He, Y.-J. Chen, V. Makhijani, G. T. Roth, X. Gomes, K. Tartaro, F. Niazi, C. L. Turcotte, G. P. Irzyk, J. R. Lupski, C. Chinault, X.-Z. Song, Y. Liu, Y. Yuan, L. Nazareth, X. Qin, D. M. Muzny, M. Margulies, G. M. Weinstock, R. A. Gibbs, and J. M. Rothberg, *Nature* **452**, 872 (2008).

[53] J. Guo, L. Yu, N. J. Turro, and J. Ju, *Acc. Chem. Res.* **43**, 551 (2010).

[54] M. Margulies, M. Egholm, W. E. Altman, S. Attiya, J. S. Bader, L. A. Bemben, J. Berka, M. S. Braverman, Y.-J. Chen, Z. Chen, S. B. Dewell, L. Du, J. M. Fierro, X. V. Gomes, B. C. Godwin, W. He, S. Helgesen, C. H. Ho, G. P. Irzyk, S. C. Jando, M. L. I. Alenquer, T. P. Jarvie, K. B. Jirage, J.- B. Kim, J. R. Knight, J. R. Lanza, J. H. Leamon, S. M. Lefkowitz, M. Lei, J. Li,

K. L. Lohman, H. Lu, V. B. Makhijani, K. E. McDade, M. P. McKenna, E. W. Myers, E. Nickerson, J. R. Nobile, R. Plant, B. P. Puc, M. T. Ronan, G. T. Roth, G. J. Sarkis, J. F. Simons, J. W. Simpson, M. Srinivasan, K. R. Tartaro, A. Tomasz, K. A. Vogt, G. A. Volkmer, S. H. Wang, Y. Wang, M. P. Weiner, P. Yu, R. F. Begley, and J. M. Rothberg, *Nature* **437**, 376 (2005).

[55] P. Bergveld, *IEEE Trans. Biomed. Eng.* **BME-17**, 70 (1970).

[56] P. Bergveld, *Sens. Actuators B* **88**, 1 (2003).

[57] J. M. Rothberg, W. Hinz, T. M. Rearick, J. Schultz, W. Mileski, M. Davey, J. H. Leamon, K. Johnson, M. J. Milgrew, M. Edwards, J. Hoon, J. F. Simons, D. Marran, J. W. Myers, J. F. Davidson, A. Branting, J. R. Nobile, B. P. Puc, D. Light, T. A. Clark, M. Huber, J. T. Branciforte, I. B. Stoner, S. E. Cawley, M. Lyons, Y. Fu, N. Homer, M. Sedova, X. Miao, B. Reed, J. Sabina, E. Feierstein, M. Schorn, M. Alanjary, E. Dimalanta, D. Dressman, R. Kasinskas, T. Sokolsky, J. A. Fidanza, E. Namsaraev, K. J. McKernan, A. Williams, G. T. Roth, and J. Bustillo, *Nature* **475**, 348 (2011).

[58] K. Mullis, F. Faloona, S. Scharf, R. Saiki, G. Horn, and H. Erlich, *Cold Spring Harb. Symp. Quant. Biol.* **51**, 263 (1986).

[59] Y. Kong, *J. Comput. Biol.* **16**, 817 (2009).

[60] D. Branton, D. W. Deamer, A. Marziali, H. Bayley, S. A. Benner, T. Butler, M. D. Ventra, S. Garaj, A. Hibbs, X. Huang, S. B. Jovanovich, P. S. Krstic, S. Lindsay, X. S. Ling, C. H. Mastrangelo, A. Meller, J. S. Oliver, Y. V. Pershin, J. M. Ramsey, R. Riehn, G. V. Soni, V. Tabard-Cossa, M. Wanunu, M. Wiggin, and J. A. Schloss, *Nat. Biotechnol.* **26**, 1146 (2008).

[61] A. Meller, L. Nivon, and D. Branton, *Phys. Rev. Lett.* **86**, 3435 (2001).

[62] A. H. Laszlo, I. M. Derrington, B. C. Ross, H. Brinkerhoff, A. Adey, I. C. Nova, J. M. Craig, K. W. Langford, J. M. Samson, R. Daza, K. Doering, J. Shendure, and J. H. Gundlach, *Nat. Biotechnol.* **32**, 829 (2014).

[63] D. Lubensky and D. Nelson, *Biophys. J.* **77**, 1824 (1999).

[64] C. T. A. Wong and M. Muthukumar, *J. Chem. Phys.* **128**, 154903 (2008).

[65] M. Muthukumar, *Polymer Translocation*, CRC, Boca Raton, FL, 2011.

[66] C. T. A. Wong and M. Muthukumar, *J. Chem. Phys.* **133**, 045101 (2010).

[67] A. S. Panwar and M. Muthukumar, *J. Am. Chem. Soc.* **131**, 18563 (2009).

[68] T. Z. Butler, M. Pavlenok, I. M. Derrington, M. Niederweis, and J. H. Gundlach, *Proc. Natl. Acad. Sci. USA* **105**, 20647 (2008).

[69] G. F. Schneider, S. W. Kowalczyk, V. E. Calado, G. Pandraud, H. W. Zandbergen, L. M. K. Vandersypen, and C. Dekker, *Nano Lett.* **10**, 3163 (2010).

[70] C. Sathe, X. Zou, J. P. Leburton, and K. Schulten, *ACS Nano* **5**, 8842 (2011).

[71] J. Clarke, H. C. Wu, L. Jayasinghe, A. Patel, S. Reid, and H. Bayley, *Nature* **4**, 265-270 (2009).

[72] J. J. Kasianowicz, J. W. F. Robertson, E. R. Chan, J. E. Reiner, and V. M. Stanford, *Annu. Rev. Anal. Chem.* **1**, 737 (2008).

[73] S. B. Zimmerman and A. P. Minton *Annu. Rev. Biophys. Biomol. Struct*. **22**, 27 (1993).

[74] H. –X. Zhou, G. Rivas, A. P. Minton *Annu. Rev. Biophys*. **37**, 375 (2008).

[75] E. A. J. F. Peters and Th. M. A. O. M. Barenbrug *Phys. Rev. E*. **66**, 056701 (2002).

[76] M. Bechtold, J. Vanderborght, O. Ippisch, and H. Vereecken *Water Resources Research* **47**, W10526 (2011).

[77] H. Hoteit, R. Mose, A. Younes, F. Lehmann, and Ph. Ackerer *Mathematical Geology*. **34**, 435 (2002).

[78] A. M. Berezhkovskii, A. V. Barzykin, and V. Y. Zitserman, *J. Chem. Phys.* **130**, 245104 (2009).

[79] S. Bezrukov, A. Berezhkovskii, M. Pustovoit, and A. Szabo, *J. Chem. Phys.* **113**, 8206 (2000).

[80] A. L. Vega, H. Yao, and W. Y. Gu, *Summer Bioengineering Conference*, Key Biscayne, FL, 1003 (2003).

[81] E. M. Johnson, D. A. Berk, R. K. Jain, and W. M. Deen, *Biophys. J.* **70**, 1017 (1996).

[82] P. Lundberg and P. W. Kuchel, *Magn. Reson. Med.* **37**, 44 (1997).

[83] I. H. Park, C. S. Johnson, and D. A. Gabriel, *Macromolecules* **23**, 1548 (1990).

[84] F. R. Runge, M. Hennig, F. Zhang, R. M. J. Jacobs, M. Sztucki, H. Schober, T. Seydel, and F. Schreiber, *P. Natl. Acad. Sci. USA* **108**, 11815 (2011).

[85] H. C. Berg and E. M. Purcell, *Biophys. J.* **20**, 193 (1977).

[86] E. D. Holmstrom and D. J. Nesbitt *J. Phys. Chem. Lett*. **1**, 2264 (2010).

[87] C. R. Crick, P. Albella, B. Ng, A. P. Ivanov, T. Roschuk et al. *Nano Lett*. **15**, 553 (2015).

[88] F. Nicoli, D. Verschueren, M. Klein, C. Dekker, and M. P. Jonsson *Nano Lett*. **14**, 6917 (2014).

[89] J. E. Reiner, J. W. F. Robertson, D. L. Burden, L. K. Burden, A. Balijepalli, and J. J. Kasianowicz, *J. Am. Chem. Soc.* **135**, 3087 (2013).

[90] Y. Ono and T. Shikata *J. Am. Chem. Soc.* **128**, 10030 (2006).

[91] B. Hornblower, A. Coombs, R. D. Whitaker, A. Kolomeisky, A. J. Picone, A. Meller, and M. Akeson, *Nat. Methods* **4,** 315 (2007).

[92] A. Ashkin, *Phys. Rev. Lett.* **24**, 156 (1970).

[93] A. Ashkin, J. M. Dziedzic, J. E. Bjorkholm, and S. Chu, *Opt. Lett.* **11**, 288 (1986).

[94] A. Fournier, N. Sasai, M. Nakao, and P.A. Defossez, *Br. Funct. Genomics* **11**, 251 (2012).

[95] V. R. B. Liyanage, J. S. Jarmasz, N. Murugeshan, M. R. Del Bigio, M. Rastegar, and J. R. Davie, *Biology* **3**, 670 (2014).

[96] M. J. Friez, J. R. Jones, K. Clarkson, H. Lubs, D. Abuelo, J. A. Bier, S. Pai, R. Simensen, C. Williams, P. F. Giampietro, C. E. Schwartz, and R. E. Stevenson, *Pediatrics* **118**, e1687 (2006).

[97] T. Yang, M. B. Ramocki, J. L. Neul, W. Lu, L. Roberts, J. Knight, C. S. Ward, H. Y. Zoghbi, F. Kheradmand, and D. B. Corry, *Sci. Transl. Med.* **4**, 1 (2012).

[98] K. Berg-Sorensen and H. Flyvbjerg, *Rev. Sci. Instrum.* **75,** 594 (2004).

[99] F. Gittes and C. Schmidt, *Method. Cell. Biol.* **55**, 129 (1998).